AD-A166 823 THE EFFECTS OF NON-SPHERICITY AND RADIATIVE ENERGY LOSS 1/1
ON THE MIGRATION O..(U) DEFENCE RESEARCH ESTABLISHMENT
VALCARTIER (QUEBEC) K C HEATON 1986

UNCLASSIFIED F/G 20/4 NL

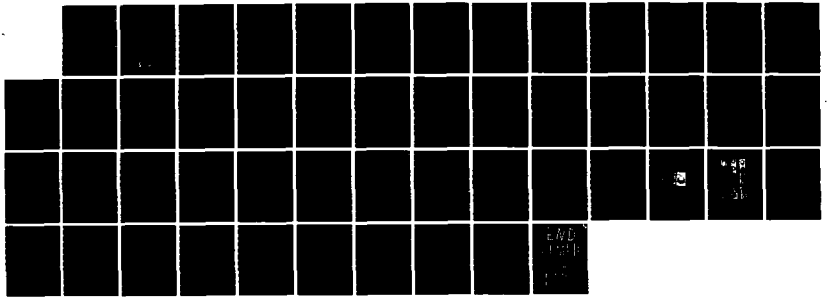

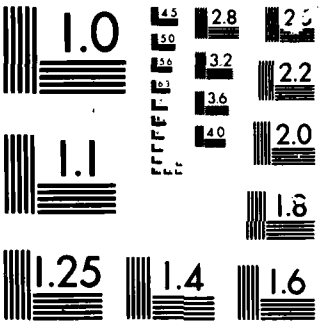

MICROCOPY CHART

THE EFFECTS OF NON-SPHERICITY AND RADIATIVE ENERGY LOSS ON THE MIGRATION OF THE GAS BUBBLE FROM UNDERWATER EXPLOSIONS

K.C. Heaton
Weapon Systems Section, Armaments Division
Defence Research Establishment Valcartier
P.O. Box 8800, Courcelette
Quebec, GOA 1RO

1986

ABSTRACT

One of the more important phenomena associated with the upward motion of a gas bubble from an underwater explosion is the significant departure from sphericity near the times of the minimum bubble radius. Neglecting this change in shape results in the prediction of a much faster upward velocity than actually occurs. The inclusion of this effect in the equations of motion has been exceedingly difficult because of the large magnitude of the departure from sphericity.

In this work, the shape of the bubble is described by an ellipsoid whose axes are allowed to vary independently, thus modelling, to first order, the changes of bubble shape. The Lagrangian equations of motion, incorporating the effects of the change of shape and of energy loss by the radiation of sound, are derived and solved for the case of a spheroidal bubble. The results of these calculations for various initial conditions are compared with analgous cases for a spherical bubble.

It is found that the spheroidal bubble model predicts a reduction in the upward translational motion of the bubble of a factor of approximately 2. A comparison of the predicted upward motion of a spheroidal bubble produced by 227.27 kg. of TNT detonated 46 metres below the surface shows good agreement with that which has actually observed.

I. INTRODUCTION

The formation of a bubble of gaseous detonation products always accompanies an underwater explosion. This bubble rises toward the surface of the water, responding as it does so to the change in the external pressure distribution with oscillatory motion, during the course of which it loses some of its energy through the emission of sonic pulses. Although the bubble is initially spherical, the effect of its upward motion is to distort it into a non-spherical shape, which becomes most pronounced in the neighbourhood of the minimum radius. The alteration in the bubble's shape further affects both the pulsations and the upward translational motion of the bubble. By means of finite element techniques, the equations of motion of the bubble can be solved, taking into account the effects of the changing shape of the bubble, although the amount of computing time required by this method limits its utility. Finite element methods have a further disadvantage in that physical insights into the systems considered are rather more difficult to come by than might otherwise have been the case.

Herring (1942) and others (eg. Taylor (1942) and Shiffman and Friedman (1944)) have treated the problem of the motion of the bubble by considering it to be a perfect sphere throughout its entire motion. This treatment yields values for the periods of radial pulsations of the bubble which are in good agreement with experimental data, but predicts a much more rapid movement toward the surface than is actually observed. This arises because the largest upward velocities of the bubble occur at those times when the bubble is near its minimum radius; it is precisely then that the largest departures from sphericity occur. Penney and Price (1942) and Ward (1943) included the effects of the non-sphericity of the bubble on its motion. However, it was always explicitly assumed in their derivations of the velocity potential of the flow about the bubble that the departures from sphericity are always small. Accordingly, their equations are not applicable near the times at which the bubble is at its smallest volumes.

Hicks (1972) was able to bring the value for the upward translational velocity of a spherical bubble at a minimum radius into agreement with experimental data by adding a drag term to the equations of motion. In his formulation, the drag coefficient is an empirical correction whose value is chosen to make the predicted rate of rise at the first minimum radius consistent with observation. However, a different drag coefficient must be selected for each charge mass and depth, requiring a comprehensive data base from which the appropriate value can be chosen for each case. For these reasons, a model for the bubble in which large deviations from sphericity and their effects on its translational motion are treated would be of considerable practical and theoretical interest.

In this work, a Lagrangian is derived for a bubble whose shape is not constrained to be always spherical but may become ellipsoidal as it moves upwards. The equations of motion for a general ellipsoidal bubble, incorporating the effects of loss of energy by radiation, are presented. The algorithm by which these equations of motion were solved numerically is briefly discussed. Computational results for some charge masses and depths are presented and compared with experimental data.

II. REVIEW OF PREVIOUS WORK

Taylor (1942) derived equations describing the motion of a spherical bubble of gas undergoing both radial pulsations and translational motion toward the water surface. These are:

$$2\pi\rho a^3\left(\frac{da}{dt}\right)^2 + \frac{\pi}{3}\rho a^3 U^2 + \frac{4\pi}{3}a^3\rho g z \qquad [2.1]$$

$$= Y_o - E(a)$$

$$U = -\frac{dz}{dt} = \frac{2g}{a^3}\int_o^t a^3 dt \qquad [2.2]$$

where a is the radius of the bubble as a function of the time t, U its upward velocity, z the position of the bubble below the pressure datum (i.e. below the zero pressure level), E(a) the internal energy of the gas comprising the bubble, g the gravitational acceleration, Y_o the total energy of the bubble and ρ the density of the water. In Taylor's formulation, there was no mechanism included for energy loss, and hence Y_o was taken to be a constant. For TNT explosions, it has been found (Herring 1942) that approximately 50% of the total explosion energy is retained by the bubble; in that case,

$$Y_o = (1.85 \times 10^{10})M \qquad [2.3]$$

where Y_o is measured in ergs, and M, the original mass of the explosive charge, is given in gm. If one assumes that the gaseous explosion products obey the ideal gas law, then the internal pressure, P, is given by

$$P = k(\rho_g)^\gamma \qquad [2.4]$$

where ρ_g is the density of the explosion products and γ the ratio of specific heats. Assuming that the entire mass, M, of the explosive has been converted to gas,

$$\rho_g = \frac{M}{(\frac{4\pi}{3})\,a^3} \qquad [2.5]$$

and hence,

$$E(a) = \int_a^\infty PdV \qquad [2.6]$$

$$= \frac{kM^\gamma a^{-3(\gamma-1)}}{(\gamma-1)\left(\frac{4\pi}{3}\right)^{\gamma-1}}$$

where $dV = 4\pi a^2 da$. Taylor, using the work of Jones, set

$$k = 7.83 \times 10^9 \qquad [2.7]$$

$$\gamma = 1.25$$

for TNT where, in eq. [2.6], E(a) is measured in ergs and m in gm.

Hicks (1972) incorporated a drag force, F_D, into the equations of motion, where F_D is given by

$$F_D = \frac{1}{2} C_D \pi \rho a^2 U^2 \qquad [2.8]$$

and the value of the drag coefficient, C_D, was chosen to be $C_D = 2.25$ in order to bring the distance travelled upward by the bubble at its first maximum into agreement with that actually observed for 500 lbs. of TNT detonated 150 ft. below the surface. By differentiating eq. [2.2], he obtained the rate of change of momentum with respect to time. The incorporation of F_D into the equation of motion yielded:

$$\frac{d}{dt}(a^3 U) = 2a^3 g - \frac{3}{4} C_D a^2 U^2 \qquad [2.9]$$

L, the Lagrangian of the bubble, is given by

$$L = 2\pi\rho a^3 \left(\frac{da}{dt}\right)^2 + \frac{\pi}{3} \rho a^3 U^2 - \frac{4\pi}{3} a^3 \rho g z \qquad [2.10]$$

$$- E(a)$$

Hence, a more general form for the equations of motion of a spherical bubble is given by

$$\frac{d}{dt}\left(\frac{\partial L}{\partial \dot{a}}\right) - \frac{\partial L}{\partial a} = Q_a,$$

$$\frac{d}{dt}\left(\frac{\partial L}{\partial \dot{z}}\right) - \frac{\partial L}{\partial z} = Q_z \qquad [2.11]$$

where $\dot{a} = \frac{da}{dt}$, $\dot{z} = \frac{dz}{dt} = -U$, and the Q_i are the generalised dissipative forces.

The dissipative drag force, Q_z, is given by F_D in eq. [2.8]. It has previously been shown (Heaton 1984) that Q_a, the generalised force for dissipation by radiation of sound, is given by

$$Q_a = -16\pi\rho a^2 \frac{\dot{a}^3}{C_S} - \frac{1}{C_S}\Delta Q_a \qquad [2.12]$$

where

$$\Delta Q_a = 4\pi\rho a^2[4a\dot{a}\ddot{a}^{\cdot} + (a^2\ddot{a}^{\cdot 2}/\dot{a})] \qquad [2.13]$$

$\ddot{a} = \frac{d^2a}{dt^2}$, and C_S is the speed of sound in the water.

The terms contained in ΔQ_a are analogous to the radiation reaction terms in electromagnetic theory, and hence can be ignored in a first approximation, although this approach will underestimate the energy loss near the minimum radius, and overestimate it elsewhere.

Ward (1943) and Penney and Price (1942) derived equations of motion for a nearly spherical bubble by expanding the velocity potential, Φ, of the flow about the bubble in terms of the Legendre polynomials, P_n, thusly:

$$\Phi = \frac{A}{r} + B_1 \frac{P_1(\cos\theta)}{r^2} + B_2 \frac{P_2(\cos\theta)}{r^3} + \ldots \qquad [2.14]$$

where the coefficients A, B_1 and B_2 are functions only of time. They further assumed that the radius vector, R(t), from the centre of the bubble to a point on its surface could be written as

$$R(t) = a + b_2P_2(\cos\theta) + b_3P_3(\cos\theta) + \ldots \qquad [2.15]$$

where a, b_2, and b_3 are functions of time only. At the surface of the bubble,

$$\frac{dR}{dt} = -\left(\frac{\partial\Phi}{\partial r}\right)_R - U\cos\theta \qquad [2.16]$$

$$= \frac{A}{R^2} + 2\frac{B_1}{R^3}P_1(\cos\theta) + 3\frac{B_2}{R^4}P_2(\cos\theta)$$

Substituting eq. [2.15] into eq. [2.16] and equating the coefficients of the Legendre polynomials on both sides of the equation yields:

$$A = a^2\frac{da}{dt},$$

$$B_1\left(1 - \frac{6}{5}\frac{b_2}{a}\right) = \frac{1}{2}a^3U, \qquad [2.17]$$

$$\frac{db_2}{dt} + 2\frac{A}{a^3}b_2 = 3\frac{B_2}{a^4}$$

$$\frac{db_3}{dt} + 2\frac{A}{a^3}b_3 = 4\frac{B_3}{a^5} - \frac{18}{5}\frac{B_1}{a^4}b_2$$

At the surface of the bubble, the pressure must be uniform and equal to the internal gas pressure. Using Bernoulli's equation, this condition can be written as

$$gz - gR\cos\theta + \left(\frac{\partial\Phi}{\partial t}\right)_R - \frac{1}{2}(\nabla\Phi)^2_R = \frac{k}{\rho}(\rho g)^\gamma \qquad [2.18]$$

If one substitutes for Φ and R in eq. [2.18], using eqs. [2.14] - [2.15], multiplies the resulting equation in turn by each of the Legendre polynomials, and then integrates over $\cos\theta$, the orthogonality relations among the Legendre polynomials produce 4 differential equations:

$$gz + a\left(\frac{d^2a}{dt^2}\right) + \frac{3}{2}\left(\frac{da}{dt}\right)^2 - \frac{U^2}{4} + O(U^4) = \frac{k}{\rho}(\rho_g)^\gamma.$$

$$\frac{1}{2}\frac{d}{dt}(a^3U) - \frac{6}{5}\int_0^t \frac{B_2}{a^2}\,dt' + O(U^3) = ga^3, \qquad [2.19]$$

$$\frac{1}{a^3}\frac{dB_2}{dt} - \frac{3B_2}{a^4}\frac{da}{dt} + \frac{3}{4}U^2 - \frac{1}{a^2}\frac{d^2a}{dt^2}\int_0^t \frac{3B_2}{a^2}\,dt'$$

$$+ O(U^3) = 0,$$

$$\frac{1}{a^4}\frac{dB_3}{dt} - \frac{4B_3}{a^5}\frac{da}{dt} - \frac{1}{a^2}\frac{d^2a}{dt^2}\int_0^t \frac{4B_3}{a^3}\,dt' + O(U^3) = 0$$

Ward (1943) has estimated the value of b_2, which measures the departures from sphericity, in eq. [2.15], and found that it remains small until the bubble begins to contract. Near the bubble's minimum radius, b_2 becomes greater than a, making the whole calculation invalid.

III. EQUATIONS OF MOTION FOR AN ELLIPSOIDAL BUBBLE

Now, let a, b, c be the semi-axes of an ellipsoid along the x, y, z axes, respectively, for a co-ordinate system whose origin is at the centre of the ellipsoid. Let the ellipsoid be immersed in a fluid of infinite extent, and let one of the axes, say a, vary with respect to time. At any instant in time, the equation of the ellipsoid will be given by

$$\frac{x^2}{a^2} + \frac{y^2}{b^2} + \frac{z^2}{c^2} = 1 \qquad [3.1]$$

The velocity potential, Φ, for the flow about the ellipsoid is given by the solution to Laplace's equation,

$$\nabla^2\Phi = 0 \qquad [3.2]$$

with appropriate boundary conditions. Since the problem obviously possesses ellipsoidal symmetry, it is most convenient to transform to ellipsoidal co-ordinates, thusly:

$$x^2 = \frac{(a^2+\lambda)(a^2+\mu)(a^2+\nu)}{(a^2-b^2)(a^2-c^2)},$$

$$y^2 = \frac{(b^2+\lambda)(b^2+\mu)(b^2+\nu)}{(b^2-c^2)(b^2-a^2)}, \qquad [3.3]$$

$$z^2 = \frac{(c^2+\lambda)(c^2+\mu)(c^2+\nu)}{(c^2-a^2)(c^2-b^2)},$$

where λ, μ, ν, are the ellipsoidal co-ordinates. The surfaces defined by λ = constant, μ = constant, ν = constant, are confocal quadrics. Because of the symmetry which exists in the transformation equations, eq. [3.3], one is allowed to specify which co-ordinate's constancy will yield confocal ellipsoids. Throughout this paper, then, the relation λ = constant will be taken to describe the family of confocal ellipsoids. In ellipsoidal co-ordinates, Laplace's equation, eq. [3.2], is given by:

$$(\mu-\nu)\left(k_\lambda \frac{\partial}{\partial\lambda}\right)^2\Phi + (\nu-\lambda)\left(k_\mu \frac{\partial}{\partial\mu}\right)^2\Phi \qquad [3.4]$$

$$+ (\lambda-\mu)\left(k_\nu \frac{\partial}{\partial\nu}\right)^2\Phi = 0$$

where k_λ is given by

$$k_\lambda = \left((a^2+\lambda)(b^2+\lambda)(c^2+\lambda)\right)^{\frac{1}{2}} \qquad [3.5]$$

and the expressions for k_μ and k_λ can be obtained from eq. [3.5] by symmetry.

Now, let α be a solution to eq. [3.4], and let another solution be given by

$$\Phi = \alpha\chi(\lambda) \qquad [3.6]$$

where χ is a function of λ only. By substituting eq. [3.6] into eq. [3.4], one finds that α must have the form

$$\alpha = \alpha_\lambda f(\mu,\nu) \qquad [3.7]$$

where α_λ is a function of λ, only (Milne-Thompson 1949). Using eq. [3.6] to aid in the solution of eq. [3.4], one finds that

$$\chi(\lambda) = A \int \frac{d\lambda}{\alpha_\lambda^2 k_\lambda} + B \qquad [3.8]$$

where A and B are arbitrary constants. Hence, if α is a solution to eq. [3.2],

$$\Phi = \alpha \int \frac{d\lambda}{\alpha_\lambda^2 k_\lambda} \qquad [3.9]$$

is also a solution. The solutions to eq. [3.4] having the form of eq. [3.9] are the ellipsoidal harmonics.

In the case of the spherical bubble, Taylor and Herring assumed that its pulsations would be described by simple radial oscillations. Since a sphere is a degenerate ellipsoid, it would be reasonable to choose as a solution to eq. [3.4] the ellipsoidal harmonic which produces analogous oscillations. Such a velocity potential is:

$$\Phi = A \int_{\lambda}^{\infty} \frac{d\lambda}{k_\lambda} \qquad [3.10]$$

since $\alpha_\lambda = 1$ is a solution to eq. [3.4]. The upper limit of the integral has been chosen in order that the potential become 0 at an infinite distance from its source. The constant of integration A is determined by the boundary conditions. Now, the boundary conditions for a pulsating ellipsoid are not as obvious as those for a sphere. Nonetheless, it seems apparent that at that point on an axis which is on the surface of the elllipsoid, the normal velocity of the fluid must be equal to the rate of change with respect to time of that axis.

Hence, for an ellipsoid in which only one axis is allowed to vary, say a,

$$\left.\frac{\partial\Phi}{\partial n}\right)_{\substack{x=a\\y=o\\z=o}} = -\dot{a} \qquad [3.11]$$

where $\dot{a} = \frac{da}{dt}$, $\frac{\partial\Phi}{\partial n} = \vec{\nabla}\Phi\cdot\hat{n}$ is the normal derivative of the potential, and $\hat{n}$ is the unit outward normal to the ellipsoid. In ellipsoidal coordinates, eq. [3.11] can be written as:

$$\left.\frac{2\,abc}{(\mu\nu)^{\frac{1}{2}}}\frac{A}{k_\lambda}\right)_{\substack{x=a\\y=o\\z=o}} = \dot{a} \qquad [3.12]$$

where the potential Φ is given by eq. [3.10].

Now, at x=a, y=o, z=o

$$\begin{aligned}\lambda &= o\\ \mu &= -b^2\\ \nu &= -c^2\end{aligned} \qquad [3.13]$$

and

$$k_\lambda = abc \qquad [3.14]$$

Hence,

$$A = \frac{1}{2}\,\dot{a}bc \qquad [3.15]$$

and

$$\Phi = \frac{1}{2}\,\dot{a}bc \int_{\lambda}^{\infty} \frac{d\lambda}{k_\lambda} \qquad [3.16]$$

The kinetic energy of the fluid around the ellipsoid is given by

$$T = -\frac{1}{2}\,\rho \oint\!\!\oint \frac{\partial \Phi}{\partial n}\,\Phi dS \qquad [3.17]$$

where the integral is carried out over a bounding ellipsoid described by eq. [3.1], and over a second outer boundary which is obtained by allowing λ in eq. [3.3] to approach infinity, essentially describing an infinitely extended ellipsoid. The contribution to eq. [3.17] from the large ellipsoid vanishes, leaving only that at the inner surface i.e. the bubble itself. The surface integral can be transformed into one over the x-y plane, thusly:

$$\oint\!\!\oint \Phi\,\frac{\partial \Phi}{\partial n}\,dS = \iint \Phi\,\frac{\partial \Phi}{\partial n}\,\frac{1}{(\hat{n}\cdot\hat{z})}\,dx\,dy \qquad [3.18]$$

where $\hat{z}$ is the unit normal along the z axis. The unit normal, $\hat{n}$, to the surface of the ellipsoid is given by

$$\hat{n} = \frac{1}{\left(\frac{x^2}{a^4} + \frac{y^2}{b^4} + \frac{z^2}{c^4}\right)^{\frac{1}{2}}}\left(\frac{x}{a^2}\,\hat{x} + \frac{y}{b^2}\,\hat{y} + \frac{z}{c^2}\,\hat{z}\right) \qquad [3.19]$$

in the ellipsoidal co-ordinates,

$$\left(\frac{\partial \Phi}{\partial n}\right)_{\lambda=o} = \frac{1}{h_1}\left(\frac{\partial \Phi}{\partial \lambda}\right)_{\lambda=o} \qquad [3.20]$$

where

$$h_1^2 = \frac{1}{4}\left(\frac{x^2}{(a^2+\lambda)^2} + \frac{y^2}{(b^2+\lambda)^2} + \frac{z^2}{(c^2+\lambda)^2}\right) \qquad [3.21]$$

So, at the surface of the ellipsoid, λ=o,

$$\frac{\partial \Phi}{\partial n} = -\frac{1}{\left(\frac{x^2}{a^4} + \frac{y^2}{b^4} + \frac{z^2}{c^4}\right)^{\frac{1}{2}}}\left(\frac{\dot{a}}{a}\right) \qquad [3.22]$$

Using eqs. [3.16], [3.18], [3.19], and [3.22] and taking account of the contributions from the half surfaces above and below the x-y plane, eq. [3.17] becomes

$$T = \frac{1}{2}\frac{cb\,\dot{a}^2}{a}\int_0^\infty \frac{d\lambda}{k_\lambda}\int_{-a}^{a}\int_{b(1-\frac{x^2}{a^2})^{\frac{1}{2}}}^{b(1-\frac{x^2}{a^2})^{\frac{1}{2}}} \frac{c^2}{z}\,dx\,dy \qquad [3.23]$$

where

$$z = c(1-\frac{x^2}{a^2}-\frac{y^2}{b^2})^{\frac{1}{2}} \qquad [3.24]$$

Evaluating eq. [3.23] finally yields the expression for the kinetic energy, T, of the flow about an ellipsoid, described by eq. [3.1], when the semi-axis a is allowed to vary with respect to time:

$$T = \pi\rho\dot{a}^2b^2c^2\int_0^\infty \frac{d\lambda}{k_\lambda} \qquad [3.25]$$

Since the equations are symmetrical with respect to all three semi-axes, it is possible to obtain expressions for the kinetic energy of the flow about an ellipsoid when each of the other semi-axes are varying by means of cyclic permutations of a, b, and c, thusly:

$$T = \pi\rho a\dot{b}^2c^2\int_0^\infty \frac{d\lambda}{k_\lambda} \qquad [3.26]$$

$$T = \pi\rho a^2b\dot{c}^2\int_0^\infty \frac{d\lambda}{k_\lambda} \qquad [3.27]$$

where $\dot{b} = \frac{db}{dt}$ and $\dot{c} = \frac{dc}{dt}$.

Hence, by adding eqs. [3.25] - [3.27], and renormalizing, one can obtain the kinetic energy, T, for the flow around an ellipsoid when all three axes are allowed to vary in time:

$$T = \frac{\pi\rho}{3}(\dot{a}^2b^2c^2 + a^2\dot{b}^2c^2 + a^2b^2\dot{c}^2)\int_0^\infty \frac{d\lambda}{k_\lambda} \qquad [3.28]$$

The normalisation factor 3 has been chosen so that eq. [3.28] is in agreement with the term for the kinetic energy due to radial spherical pulsations in eq. [2.1] when a=b=c and $\dot{a}=\dot{b}=\dot{c}$.

As mentioned above, it is not entirely clear what sort of boundary conditions are applicable at the surface of a pulsating ellipsoid. In fact, the specification of boundary conditions when all three semi-axes are varying is equivalent to putting constraints on the interactions among $\dot{a}$, $\dot{b}$, and $\dot{c}$, which, in turn, is equivalent to specifying which shapes the bubble will be allowed to assume. Equation [3.28] corresponds to a velocity potential which has been so constructed that the velocity cross-terms in eq. [3.17] cancel out. Since $\dot{a}$, $\dot{b}$, and $\dot{c}$, are all mutually perpendicular, this seems physically reasonable. This has the effect of insisting that the movement of a point on an axis of the ellipsoid is due only to the change in length of that axis, with the changes in the lengths of the other two axes contributing nothing.

The velocity potential associated with the purely translational motion of the ellipsoid along the z axis is well known (e.g. Milne-Thompson 1949). The boundary condition is

$$-\frac{\partial\Phi}{\partial n}\Big)_{\lambda=o} = U\cos\Theta_z \qquad [3.29]$$

where, as before, $-U = \frac{dz}{dt} = \dot{z}$, Θ_z is the angle between the z axis and the normal to the surface of the ellipsoid, and z is the position of the bubble centre below the pressure datum. Since

$$\cos\Theta_z = \frac{1}{h_1}\frac{\partial z}{\partial\lambda}\Big)_{\lambda=o} \qquad [3.30]$$

eq. [3.29] becomes

$$\frac{\partial\Phi}{\partial\lambda}\Big)_{\lambda=o} = -U\frac{\partial z}{\partial\lambda}\Big)_{\lambda=o} \qquad [3.31]$$

The solution to eq. [3.4] which satisfies the boundary conditions in eq. [3.31] is the first order ellipsoidal harmonic given by

$$\Phi = Cz\int_{\lambda}^{\infty}\frac{d\lambda}{(c^2+\lambda)k_\lambda} \qquad [3.32]$$

where C is a constant of integration. Direct substitution of eq. [3.32] back into eq. [3.31] yields

$$C = -\frac{abc\ U}{2-\alpha_o} \qquad [3.33]$$

where

$$\alpha_o = abc\int_{o}^{\infty}\frac{d\lambda}{(c^2+\lambda)k_\lambda} \qquad [3.34]$$

The kinetic energy of the flow around a translating ellipsoid is then given by:

$$\begin{aligned} T &= -\frac{1}{2}\rho\iint\Phi\frac{\partial\Phi}{\partial n}\,dS \\ &= \frac{\alpha_o}{2(2-\alpha_o)}\rho U^2\iint z\cos\Theta_z dS \qquad [3.35] \\ &= \frac{2\pi}{3}abc\rho\left(\frac{\alpha_o}{2-\alpha_o}\right)U^2 \end{aligned}$$

As before, the integration is carried out over a bounding ellipsoid whose semi-axes are a, b, and c, and over one whose semi-axes are allowed to extend to infinity, where the contribution from the outer ellipsoid vanishes. Hence, the kinetic energy for the flow generated by a translating ellipsoid whose semi-axes are varying in time is given by:

$$T = \frac{\pi\rho}{3}(\dot{a}^2b^2c^2 + a^2\dot{b}^2c^2 + a^2b^2\dot{c}^2)\int_0^\infty \frac{d\lambda}{k_\lambda} \qquad [3.36]$$

$$+ \frac{2\pi}{3}\,abc\rho\left(\frac{\alpha_o}{2-\alpha_o}\right)U^2$$

Equation [3.36] has no provision for the interaction of $\dot{a}$, $\dot{b}$, or $\dot{c}$ with U. Again, this is not unexpected since eq. [3.35] should yield the kinetic energy terms in eq. [2.1], as it does in fact do, when a=b=c and $\dot{a}=\dot{b}=\dot{c}$. Physically, as long as the bubble is symmetrical with respect to the x-y plane, the contributions from the top and bottom halves to a coupling of the oscillatory motion with the translational exactly cancel each other.

The energy, V_p, associated with the hydrostatic pressure around the bubble is:

$$V_p = \frac{4\pi}{3}\,\rho gabcz \qquad [3.37]$$

The internal energy of the bubble, E(a,b,c), is given by

$$E(a,b,c) = \frac{kM\gamma a^{-(\gamma-1)}b^{-(\gamma-1)}c^{-(\gamma-1)}}{(\gamma-1)\left(\frac{4\pi}{3}\right)^{\gamma-1}} \qquad [3.38]$$

Hence, the Lagrangian, L, for the flow around an ellipsoidal bubble whose semi-axes are a, b, c, at a depth z below the pressure datum, where the z axis is parallel to the ellipsoid axis c, and which is moving with a translational velocity $U = -\frac{dz}{dt}$ is given by

$$L = \frac{\pi}{3}\rho(\dot{a}^2b^2c^2 + a^2\dot{b}^2c^2 + a^2b^2\dot{c}^2)\int_0^\infty \frac{d\lambda}{k_\lambda}$$

$$+ \frac{2\pi}{3}\,\rho abc\left(\frac{\alpha_o}{2-\alpha_o}\right)U^2 - \frac{4\pi}{3}\,\rho abcgz \qquad [3.39]$$

$$- \frac{kM\gamma a^{-(\gamma-1)}b^{-(\gamma-1)}c^{-(\gamma-1)}}{(\gamma-1)\left(\frac{4\pi}{3}\right)^{\gamma-1}}$$

The total energy of the bubble, Y(t), at any time t is therefore given by:

$$Y(t) = \frac{\pi}{3}\rho(\dot{a}^2b^2c^2 + a^2\dot{b}^2c^2 + a^2b^2\dot{c}^2)\int_0^\infty \frac{d\lambda}{k_\lambda}$$

$$+ \frac{2\pi}{3}\,\rho abc\left(\frac{\alpha_o}{2-\alpha_o}\right)U^2 + \frac{4\pi}{3}\,\rho abcgz \qquad [3.40]$$

$$+ \frac{kM\gamma a^{-(\gamma-1)}b^{-(\gamma-1)}c^{-(\gamma-1)}}{(\gamma-1)\left(\frac{4\pi}{3}\right)^{\gamma-1}}$$

Hence, the equations of motion for the bubble are:

$$\frac{d}{dt}\left(\frac{\partial L}{\partial \dot{a}}\right) - \frac{\partial L}{\partial a} = Q_a,$$

$$\frac{d}{dt}\left(\frac{\partial L}{\partial \dot{b}}\right) - \frac{\partial L}{\partial b} = Q_b, \qquad [3.41]$$

$$\frac{d}{dt}\left(\frac{\partial L}{\partial \dot{c}}\right) - \frac{\partial L}{\partial c} = Q_c,$$

$$\frac{d}{dt}\left(\frac{\partial L}{\partial \dot{z}}\right) - \frac{\partial L}{\partial z} = Q_z,$$

where the Q_i are the generalised dissipative forces.

The substitution of eq. [3.39] into eq. [3.41] results in:

$$\begin{aligned}
\frac{2\pi}{3}\rho b^2c^2I_o\ddot{a} = &-\frac{2\pi}{3}\rho\left[b^2c^2\frac{\partial I_o}{\partial a}\dot{a}^2\right.\\
&\left.+\left(2c^2bI_o + b^2c^2\frac{\partial I_o}{\partial b}\right)\dot{a}\dot{b} + \left(2b^2cI_o + b^2c^2\frac{\partial I_o}{\partial c}\right)\dot{a}\dot{c}\right]\\
&+\frac{\pi}{3}\rho(\dot{a}^2b^2c^2 + a^2\dot{b}^2c^2 + a^2b^2\dot{c}^2)\frac{\partial I_o}{\partial a}\\
&+\frac{2\pi}{3}\rho(ac^2\dot{b}^2 + ab^2\dot{c}^2)I_o + \frac{2\pi}{3}\rho bcf(\alpha_o)\dot{z}^2\\
&+\frac{2\pi}{3}\rho abc\frac{\partial f(\alpha_o)}{\partial a}\dot{z}^2 - \frac{4\pi}{3}\rho gbcz\\
&+(\gamma-1)Ka^{-\gamma}b^{-(\gamma-1)}c^{-(\gamma-1)} + Q_a,
\end{aligned} \qquad [3.42]$$

$$\begin{aligned}
\frac{2\pi}{3}\rho a^2c^2I_o\ddot{b} = &-\frac{2\pi}{3}\rho\left[a^2c^2\frac{\partial I_o}{\partial b}\dot{b}^2\right.\\
&\left.+\left(2ac^2I_o + a^2c^2\frac{\partial I_o}{\partial a}\right)\dot{a}\dot{b} + \left(2a^2cI_o + a^2c^2\frac{\partial I_o}{\partial c}\right)\dot{b}\dot{c}\right]\\
&+\frac{\pi}{3}\rho(\dot{a}^2b^2c^2 + a^2\dot{b}^2c^2 + a^2b^2\dot{c}^2)\frac{\partial I_o}{\partial b}\\
&+\frac{2\pi}{3}\rho(bc^2\dot{a}^2 + ba^2\dot{c}^2)I_o + \frac{2\pi}{3}\rho acf(\alpha_o)\dot{z}^2\\
&+\frac{2\pi}{3}\rho abc\frac{\partial f(\alpha_o)}{\partial b}\dot{z}^2 - \frac{4\pi}{3}\rho gacz\\
&+(\gamma-1)Ka^{-(\gamma-1)}b^{(-\gamma)}c^{-(\gamma-1)} + Q_b,
\end{aligned} \qquad [3.43]$$

$$\frac{2\pi}{3}\rho a^2b^2I_o\ddot{c} = -\frac{2\pi}{3}\rho\left[a^2b^2\frac{\partial I_o}{\partial c}\dot{c}^2\right.$$

$$+ (2ab^2 I_o + a^2 b^2 \frac{\partial I_o}{\partial a})\dot{a}\dot{c} + (2a^2 b I_o + a^2 b^2 \frac{\partial I_o}{\partial b})\dot{b}\dot{c}\Big] \qquad [3.44]$$

$$+ \frac{\pi}{3} \rho(\dot{a}^2 b^2 c^2 + a^2 \dot{b}^2 c^2 + a^2 b^2 \dot{c}^2) \frac{\partial I_o}{\partial c}$$

$$+ \frac{2\pi}{3} \rho(\dot{a}^2 b^2 c + a^2 \dot{b}^2 c) I_o + \frac{2\pi}{3} \rho abf(\alpha_o)\dot{z}^2$$

$$+ \frac{2\pi}{3} \rho abc \frac{\partial f(\alpha_o)}{\partial c} \dot{z}^2 - \frac{4\pi}{3} \rho gabz$$

$$+ (\gamma-1)Ka^{-(\gamma-1)}b^{-(\gamma-1)}c^{-\gamma} + Q_c,$$

$$\ddot{z} = - (\frac{\dot{a}}{a} + \frac{\dot{b}}{b} + \frac{\dot{c}}{c})\dot{z} - \frac{2}{\alpha_o(2-\alpha_o)} \frac{d\alpha_o}{dt} \dot{z} \qquad [3.45]$$

$$- \frac{g}{f(\alpha_o)} + Q_z,$$

where

$$\ddot{a} = \frac{d^2 a}{dt^2}, \quad \ddot{b} = \frac{d^2 b}{dt^2}, \quad \ddot{c} = \frac{d^2 c}{dt^2},$$

$$\ddot{z} = \frac{d^2 z}{dt^2}, \qquad [3.46]$$

$$I_o = \int_o^\infty \frac{d\lambda}{k_\lambda},$$

$$f(\alpha_o) = \frac{\alpha_o}{(2-\alpha_o)},$$

$$\frac{dI_o}{dt} = \frac{\partial I_o}{\partial a} \dot{a} + \frac{\partial I_o}{\partial b} \dot{b} + \frac{\partial I_o}{\partial c} \dot{c},$$

$$\frac{df(\alpha_o)}{dt} = \frac{\partial f(\alpha_o)}{\partial a}\dot{a} + \frac{\partial f(\alpha_o)}{\partial b}\dot{b} + \frac{\partial f(\alpha_o)}{\partial c}\dot{c},$$

$$K = \frac{kM^\gamma}{(\gamma-1)(\frac{4\pi}{3})^{\gamma-1}}$$

In order to complete the derivation of the equations of motion of the bubble, it is necessary to determine Q_a, Q_b, Q_c and Q_z, the generalised dissipative forces associated with the radiation of sound by the bubble. Now, at distances large compared with the scale of the bubble, the form of the velocity potential, Φ, in the fluid will be identical with that of a spherical bubble. Hence,

$$\Phi = - \frac{C}{r} + \vec{A} \cdot \vec{\nabla}(1/r) \qquad [3.47]$$

where C and $\vec{A}$ are constants which depend only on the time t. r is the distance to the field point from an origin located somewhere within the bubble.

Following the development given by Landau and Lifshitz (1966), in the wave zone,

$$\Phi = \frac{C(t')}{r} + \vec{\nabla}\cdot\left(A(t')\ \frac{\cos\Theta}{r}\ \hat{r}\right) \qquad [3.48]$$

where Θ is the angle between the direction of the translational motion and r, and the retarded time t' is given by

$$t' = t - \frac{r}{C_S} \qquad [3.49]$$

where C_S is, as before, the velocity of sound in water. The velocity, $\vec{V}$, of the water in the wave zone must therefore be given by:

$$\vec{V} = -\vec{\nabla}\Phi$$

$$= \left(\frac{1}{C_S r}\ \frac{\partial C(t)}{\partial t} - \frac{\cos\Theta}{C_S^2 r}\ \frac{\partial^2 A(t)}{\partial t^2}\right)\hat{r} \qquad [3.50]$$

$$+\ldots$$

where terms of higher negative order in r have been neglected. The total energy emitted as sonic radiation per unit time, $\frac{dE}{dt}$ is then:

$$\frac{dE}{dt} = -\rho C_S \iint (\vec{V}\cdot\vec{V})dS$$

$$= -\frac{4\pi\rho}{C_S}\left(\frac{\partial C(t)}{\partial t}\right)^2 - \frac{4\pi\rho}{3C_S^3}\left(\frac{\partial^2 A(t)}{\partial t^2}\right)^2 \qquad [3.51]$$

where the integral has been taken over a sphere of radius r (Landau and Lifshitz 1966).

To a good approximation, the term in eq. [3.51] proportional to C_S^{-3} can be neglected for low translational velocities, since it will be 2 orders of magnitude smaller than that proportional to C_S^{-1}.

Now, the volume $4\pi C$ of fluid which flows through the surface over which the integral in eq. [3.51] is taken must be equal to the rate of change with respect to time of the volume, $\mathcal{V}$, of the bubble. Thus,

$$C = \frac{1}{4\pi}\ \dot{\mathcal{V}}$$

$$= \frac{1}{3}\left(\dot{a}bc + a\dot{b}c + abc\right) \qquad [3.52]$$

and so

$$\frac{dE}{dt} = -\frac{4\pi\rho}{9C_S}\left[\ddot{a}bc + a\ddot{b}c + ab\ddot{c}\right.$$
$$+ \dot{a}(\dot{b}c + b\dot{c})$$
$$+ \dot{b}(\dot{a}c + a\dot{c}) \qquad [3.53]$$
$$\left. + \dot{c}(\dot{a}b + a\dot{b})\right]^2$$

Now, evidently,

$$\frac{dE}{dt} = \dot{a}Q_a + \dot{b}Q_b + \dot{c}Q_c + \dot{z}Q_z \qquad [3.54]$$

Since all of the dependence on the translational velocity in eq. [3.51] was contained in the term proportional to C_S^{-3}, it follows that, to the same approximation, $Q_z = 0$ in eq. [3.54]. Since, in the absence of any translational motion, there exists nothing to distinguish one axis of the ellipsoid from another, it follows that one should be able to obtain the other two Q_i from one by cyclic permutation of the axes a, b, and c. The only grouping of the terms in eq. [3.53] which is invariant under cyclic permutation of the axes is given by

$$\frac{dE}{dt} = -\frac{4\pi}{9C_S}\rho\left[F(\ddot{a})\sum_{i=1}^{3}F(\ddot{a}_i)\right.$$
$$\left. + F(\ddot{b})\sum_{i=1}^{3}F(\ddot{a}_i) + F(\ddot{c})\sum_{i=1}^{3}F(\ddot{a}_i)\right] \qquad [3.55]$$

where

$$F(\ddot{a}_i) = \ddot{a}_i a_j a_k + \dot{a}_i \dot{a}_j a_k \qquad [3.56]$$
$$+ \dot{a}_i \dot{a}_k a_j, \quad i \neq j \neq k$$

and $a_1 = a$, $a_2 = b$, $a_3 = c$.

Hence, by comparison of eq. [3.55] with eq. [3.54],

$$Q_{a_i} = -\frac{4\pi}{9C_S}\rho\frac{F(\ddot{a}_i)}{\dot{a}_i}\sum_{j=1}^{3}F(\ddot{a}_j) \qquad [3.57]$$

where, as before, i, j, k, are successively equal to 1, 2, 3. Now, as was the case for the spherical bubble, the terms in eq. [3.57] which depend upon the products of the pulsational accelerations with themselves or with the pulsational velocities are analogous to the radiation reaction terms in electromagnetic theory. This suggests that such terms

may be ignorable, at least in a first approximation. At this stage, in the absence of any perturbing force in the x-y plane, it is possible to allow $\dot{b} = \dot{a}$. This allows one to drop eq. [3.42] as an equation of motion, and replace $\dot{b}$ and b by $\dot{a}$ and a in eqs. [3.43] - [3.45] and eq. [3.57]. This, of course, specialises the equations of motion to those of a spheroidal bubble. Henceforth, throughout this paper, the case of the spheroidal bubble will be treated exclusively.

To sum up: eqs. [3.42] - [3.45] are equations of motion describing a pulsating ellipsoidal bubble undergoing translational motion. When $Q_a = Q_b = Q_z = 0$, the equations neglect any sort of energy loss. It has been shown that the energy loss from the translational motion of the bubble can be expected to be negligible with respect to that from the pulsational motion and so Q_z was set to 0 in eq. [3.45]. It was further shown that

$$Q_{a_i} = -\frac{4\pi}{9C_S}\rho\frac{F(\dot{a}_i^3)}{\dot{a}_i}\sum_{j=1}^{3}F(\dot{a}_j^3) \qquad [3.58]$$

where

$$F(\dot{a}_i^3) = \dot{a}_i\dot{a}_j a_k + \dot{a}_i\dot{a}_k a_j + \Delta F(\dot{a}_i^3),\ i\neq j\neq k \qquad [3.59]$$

When one wishes to ignore the effects of radiation reaction,

$$\Delta F(\dot{a}_i^3) = 0 \qquad [3.60]$$

and

$$\Delta F(\dot{a}_i^3) = \ddot{a}_i a_j a_k,\ i\neq j\neq k \qquad [3.61]$$

when one wishes to include them.

IV. NUMERICAL METHODS OF SOLUTION

Before one attempts numerical solutions of the equations of motion, eqs. [3.43] - [3.45], it is useful to make them non-dimensional. Thus, the substitution of

$$\begin{aligned} a &= a^*L, \\ c &= c^*L, \\ z &= z^*L, \\ t &= t^*T \end{aligned} \qquad [4.1]$$

into the equations of motion used, where

$$L = \left(\frac{Y_o}{g\rho}\right)^{\frac{1}{4}} \qquad [4.2]$$

$$T = \sqrt{\frac{L}{g}}$$

yields a dimensionless form of the equations of motion. As before, Y_o is given by eq. [2.3] and g and ρ are, respectively, the gravitational acceleration and the density of water. These particular scaling factors in eq. [4.2] were originally used by Taylor (1942).

Since all of the equations of motion have the unfortunate property of singularity at the origin, it is necessary to begin the integration with a series solution. Taylor (1942) suggested that the initial solutions to the dimensionless forms of eqs. [2.1] - [2.2] be

$$a^* = \left(\frac{t^*}{1.0025}\right)^{2/5},$$

$$\dot{z}^* = -\left(\frac{10}{11}\right)t^*, \qquad [4.3]$$

$$z^* = z_o - \left(\frac{5}{11}\right)t^{*2},$$

where z_o^* is the initial dimensionless depth below the pressure datum, for values of t^* near zero. Since the bubble can be expected to be spherical initially, the values for a^*, $\dot{z}^*$, and z^* from eq. [4.3] were used to begin the integration at time t_o, with the additional requirement that $a^* = c^*$. One also needs initial values for the rates of change, $\dot{a}^*$ and $\dot{c}^*$, of the semi-axes. These were estimated by assuming that the bubble would be initially spherical and substituting into the dimensionless form of eq. [2.1] to find $\dot{a}^*$. Hence, the initial values for $\dot{a}^*$ and $\dot{c}^*$ are given by

$$\dot{a}^{*2} = \left(1 - \frac{E^*(a^*)}{Y_o}\right)\frac{1}{2\pi a^{*3}} - \left(\frac{\dot{z}^*}{6}\right)^2 - \frac{2}{3}z^*, \qquad [4.4]$$

$$\dot{a}^* = \dot{c}^*,$$

where

$$E^*(a^*) = \frac{kM^{\gamma}a^{*-3(\gamma-1)}}{(\gamma-1)\left(\frac{4\pi}{3}\right)^{\gamma-1}L^{3(\gamma-1)}}, \qquad [4.5]$$

Y_o is the initial total energy, as given by eq. [2.3], and all other variables are as previously defined.

Another numerical difficulty concerns the evaluation of the terms $\frac{\partial I_o}{\partial a}$, $\frac{\partial I_o}{\partial c}$, $\frac{\partial \alpha_o}{\partial a}$, $\frac{\partial \alpha_o}{\partial c}$. Now, evidently,

$$\frac{\partial I_o}{\partial a} = -a \int_o^\infty \frac{d\lambda}{(a^2+\lambda)^{3/2}\,(b^2+\lambda)^{\frac{1}{2}}\,(c^2+\lambda)^{\frac{1}{2}}},$$

$$\frac{\partial I_o}{\partial c} = -c \int_o^\infty \frac{d\lambda}{(a^2+\lambda)^{\frac{1}{2}}\,(b^2+\lambda)^{\frac{1}{2}}\,(c^2+\lambda)^{3/2}}, \qquad [4.6]$$

$$\frac{\partial \alpha_o}{\partial c} = bcI_1 + abc\,\frac{\partial I_1}{\partial a}, \qquad [4.7]$$

$$\frac{\partial \alpha_o}{\partial c} = abI_1 + abc\,\frac{\partial I_1}{\partial c}$$

where

$$I_1 = \int_o^\infty \frac{d\lambda}{(a^2+\lambda)^{\frac{1}{2}}\,(b^2+\lambda)^{\frac{1}{2}}\,(c^2+\lambda)^{3/2}} \qquad [4.8]$$

I_o and I_1 were evaluated with the IMSL double precision subroutines MMLINF and MMLIND, which compute incomplete elliptic integrals of the first and second kind, respectively. The partial derivatives of I_o, eq. [4.6], are, in fact, incomplete elliptic integrals of the second kind, and can be evaluated with MMLIND. The evaluation of the second terms in eq. [4.7] presented considerable difficulty. In point of fact, no commercial routine capable of evaluating eqs. [4.7] seems to exist, and the difficulties involved in the composition of one ab nihilo are formidable. Accordingly, as a stopgap, the terms in eqs. [4.7] which involve the derivative of an incomplete elliptic integral of the second kind were evaluated by holding one of a or c constant, and varying the other at each step in the integration, thusly:

$$\frac{\partial I_1}{\partial a} = \frac{1}{2\Delta a}\,(I_1(a+\Delta a,c) - (I_1(a-\Delta a,c)), \qquad [4.9]$$

$$\frac{\partial I_1}{\partial c} = \frac{1}{2\Delta c}\,(I_1(a,\ c+\Delta c) - I_1(a,\ c-\Delta c))$$

where MMLIND was used to evaluate I_1. Since Δa and Δc can be made as small as desired, theoretically eq. [4.9] can be made to approximate the true value of the derivative as closely as desired; however, the practical constraints of computational time, machine accuracy, and the accuracy of the IMSL subroutines do place limits on the size of Δa and Δc.

The actual integrations were carried out using a 4 point Runge-Kutta algorithm incorporating automatic error controls. Some numerical difficulties with this method were encountered when the radiation reaction was incorporated using eq. [3.61]. Near the minima of a and c, $\dot{a}$ and $\dot{c}$ become small, and change sign as well. Because of their dependence upon $\dot{a}^{-1}$ and $\dot{c}^{-1}$, the values of Q_a and Q_c can oscillate rapidly, adversely affecting the convergence of the integration. This difficulty was circumvented by the use of a series approximation in which $\dot{a}^{-1}$ and $\dot{c}^{-1}$ were replaced by averaged pulsational velocities. By using eq. [3.40], it is possible to write

$$\overline{a^{*4}}\ (\overline{\dot{a}^{*2}})I^*_o = (\frac{Y(t) - E^*(a^*)}{Y_o})\frac{3}{\pi} \qquad [4.10]$$

$$-2a^*b^*c^*(\frac{\alpha_o}{2-\alpha_o})\dot{z}^{*2} - 4a^*b^*c^*z^*$$

where

$$\overline{a^{*4}} = \frac{1}{81}(a+b+c)^4$$

$$\overline{\dot{a}^{*2}} = \frac{1}{\overline{a^{*4}}}(\dot{a}^{*2}b^{*2}c^{*2} + a^{*2}\dot{b}^{*2}c^{*2} \qquad [4.11]$$

$$+ a^{*2}b^{*2}\dot{c}^{*2})$$

and Y(t) is the energy of the bubble at any time t, given by eq. [3.40].

If one defines:

$$\alpha = (\frac{Y(t)-E^*(a^*)}{Y_o})\ \frac{3}{\pi}\ (\overline{a^{*4}})I^*_o \qquad [4.12]$$

$$\beta = -\frac{2a^*b^*c^*}{(\overline{a^{*4}})I^*_o}(\frac{\alpha_o}{2-\alpha_o})\dot{z}^{*2} - \frac{4a^*b^*c^*z^*}{(\overline{a^{*4}})I^*_o}$$

then,

$$(\overline{\dot{a}^{*2}})^{-\frac{1}{2}} = \frac{\pm 1}{\alpha^{\frac{1}{2}}}(1 + \frac{1}{2}\frac{\beta}{\alpha} + \frac{3}{8}(\frac{\beta}{\alpha})^2\ t...) \qquad [4.13]$$

where the positive value is taken while a particular axis is expanding and the negative while it is contracting. By expanding the dimensionless form of eq. [3.58] when $\Delta F(a_1)$ is given by eq. [3.61], and substituting $(\overline{\dot{a}^{*2}})^{-\frac{1}{2}}$ for $(\dot{a}^*)^{-1}$ and $(\dot{c}^*)^{-1}$, values for the dissipative function incorporating averaged radiation reaction terms were obtained.

Estimates for a and c were arrived at by the substitution of the current values of a, c, $\dot{a}$, $\dot{c}$, z, and $\dot{z}$ into eqs. [3.43] and [3.44] with Q_a and Q_c set to zero. Those values for a and c were substituted back into eq. [3.58], to obtain new values for Q_a and Q_c which were in turn used in eqs. [3.43] and [3.44] to obtain new estimates for a and c.

V. NUMERICAL RESULTS AND ANALYSIS

Figures 2-11 show the results of computations for a bubble produced by the detonation of 2.1136 kg. of TNT 6.1 metres below the surface, using eqs. [3.43] - [3.46] for a spheroidal bubble. Those curves associated with a spheroidal bubble and labelled '$\Delta Y = 0$' were calculated under the assumption of no energy loss; that is, $Q_a = Q_c = Q_z = 0$ in eqs. [3.42] - [3.46]. The curves labelled '$\Delta Y \neq 0$, $\Delta F = 0$', were

calculated incorporating radiative energy loss, but not radiation reaction terms; that is, eqs. [3.58] - [3.60] were used to define Q_a and Q_c. In Figs. 2-5, a and c are the semi-axes of the spheroidal bubble, where a is the semi-axis in the plane normal to the bubble's upward motion, and c the semi-axis in the plane parallel to the bubble's upward motion.

Taylor (1942) considered the same case, using eqs. [2.1] - [2.2] for a spherical bubble in the absence of any energy loss from any source. In Figs. 2-11, the curves labelled with '$\Delta Y = 0$' were obtained by solving eqs. [2.10] - [2.11], with $Q_a = Q_z = 0$, which are equivalent to Taylor's equations for a spherical bubble. The curves labelled '$\Delta Y \neq 0$, $\Delta Q_a = 0$' result from the incorporation of radiative energy loss, neglecting radiation reaction, into eqs. [2.10] - [2.11]; that is; Q_a was given by eq. [2.12], with $\Delta Q_a = 0$. The curves labelled '$\Delta Y \neq 0$, $\Delta Q_a \neq 0$' incorporate energy loss including radiation reaction; that is; Q_a and ΔQ_a were given by eqs. [2.12] - [2.13]. In Figs. 2-5, 'radius' refers to the spherical bubble radius as calculated in eqs. [2.10] - [2.11].

The curves labelled 'spherical' in Figs. 6-11 are the upward velocities and heights above the original detonation point, obtained by solving eqs. [2.10] - [2.11] for a spherical bubble, under different assumptions about the nature of the energy loss. The curves labelled 'spheroidal' are the same quantities obtained from the solution of eqs. [3.43] - [3.46] for a spheroidal bubble.

Taylor (1943) presented photographs showing the behaviour of bubbles generated by electrical discharges in oil, which are here reproduced in Figs. 12-13. These show that a bubble in the early stages of its motion is very nearly spherical, but that near its minimum volume, it becomes approximately disc shaped, with its longest dimension lying in the plane normal to the direction of its upward motion. Near the second maximum, the bubble is highly non-spherical, and, in fact, seems to be attempting to fission, exhibiting an extremely large bulge on its upper surface and a flat lower surface. After the bubble has passed through its second maximum, it becomes mushroom-shaped and actually does bifurcate at its second minimum. The two halves rejoin later to form a distorted disc.

As one can see from Fig. 2, a spheroidal bubble reproduces the salient features of the observed behaviour, at least qualitatively. a and c were very nearly equal to each other, as well as to the spherical radius, at the first maximum. Near the first minimum, the bubble became more obviously spheroidal, with the ratio a/c assuming a value of 2.34. After the first minimum, the qualitative agreement between the spheroidal bubble model and Taylor's photographs was less pronounced. This was hardly surprising, given that the equations of motion constrain the

possible shapes of the bubble to spheroids. However, the model does at least predict that the bubble would not return to a spherical shape. In addition, the spheroidal model also retains one of the successful features of the spherical model, that of the prediction of the period of the bubble's oscillation. The period of the first oscillation in Fig. 2 (which was defined for both the spherical and spheroidal bubble to be the time after a maximum at which the first derivative of the volume changed sign) was .26 seconds for both models. It should also be noted that the time at which the volume was a minimum did not coincide with the minima of either a or c. In Fig. 2, a reached its first minimum a full .01 seconds before c did.

Figures 3-4 show the effects of incorporating radiative energy loss into the spheroidal bubble model, and compare the results with the analogous case for a spherical bubble. When radiative energy loss was included in the calculations, the second minima of a and c occurred slightly earlier, and was more nearly coincident. Figure 5 compares the semi-axes for a spheroidal bubble under various assumptions about the form of the energy loss. It is interesting that the most noticeable difference among the calculations was in the value of c.

The outstanding failure of the spherical model for the bubble is its prediction of a too rapid rate of rise when the bubble's volume is a minimum. As Figs. 6-10 show, the maximum upward velocity predicted by the spheroidal model was less than that predicted by the spherical model by a factor of 2, and consequently the distance travelled from the site of the explosion was decreased by about the same amount. This diminuation of the upward translational velocity of the bubble near its minimum volume accounted for the differences between the periods of the spherical and spheroidal models after the first minimum in Figs. 2-4. Because the spheroidal bubble was deeper than the spherical one, the hydrostatic pressure was greater, making the period shorter. This is also the reason that the curves in Figs. 2-11 associated with the spherical bubble model terminated .1 seconds before those of the spheroidal model. Because of the spherical bubble's greater upward velocities, it reached the surface before the spheroidal one.

Figure 11 shows the energy possessed by the bubble as a function of time for both the spherical and spheroidal models. Since the initial solutions to the equations of motion for the spheroidal bubble were calculated by assuming it to have been initially spherical, it is not surprising that, in the absence of dissipation, the energies predicted by the two models were found to be constant and equal. The energy losses predicted by the spheroidal model without radiation reaction were found to be in close agreement with those of the spherical model without radiation reaction. After the first minimum volume was passed, the spheroidal model predicted a slightly greater energy loss than the spherical, until the spheroidal bubble passed through a second minimum volume.

The most dramatic difference between the spheroidal and spherical models is in the role of radiation reaction. As can be seen in Fig. 11, the inclusion of radiation reaction in the spherical bubble model decreased the amount of energy radiated. For the spheroidal bubble, this was the case only until the first minimum volume was passed. After that time, the effect of including radiation reaction in the calculation was to increase the radiative energy loss, compared both to that of the spheroidal model without radiation reaction and to that of either spherical model. Moreover, since even without the inclusion of radiation reaction, the spheroidal model yielded a greater energy loss than the analogous spherical case, it seems that this was not an artefact of the approximations used in the computation of the radiation reaction terms. Whether the magnitude of the increase in the energy loss which occurred when radiation reaction terms were added to the equations would be as large as that indicated by Fig. 11 is rather more uncertain. The close correspondence between the predicted energy losses for the spherical and spheroidal models prior to the first minimum suggests that the calculation was valid, at least in the regime in which the bubble was nearly spherical. However, as mentioned above, after the first minimum, the actual shape of the bubble is not really spheroidal. Consequently, the actual radiation loss may be quite different to that calculated for a spheroidal bubble. However, since the bubble is even less spherical than it is spheroidal, on balance, it seems probable that the predictions of the spheroidal model were more accurate than those of the spherical.

Hicks (1972) solved the equations of motion for a spherical bubble, with the addition of a hydrodynamic drag term, for 227.27 kg. of TNT at a depth of 45.73 metres below the surface. (That is, Hicks took eqs. [2.11] as his equations of motion, with Q_z as defined by eq. [2.8] and $Q_a = 0$). It has been observed that a bubble from an explosion with these characteristics rises approximately 3.35 metres from the location of the explosion in the time taken to reach its first minimum. Hicks found that where drag is the only source of dissipation, a drag coefficient of $C_D = 2.25$ had to be introduced into the equations of motion for a spherical bubble in order to reproduce this behaviour. In this work, for the initial solutions chosen, it was found that a drag coefficient of $C_D = 1.85$ brought the predicted rise of a spherical bubble into better agreement with observation. When radiative dissipation was also included, a drag coefficient of $C_D = 1.6$ yielded better agreeement with observation.

In Figs. 14-23, the curves labelled 'spherical' were obtained by taking eqs. [2.10] - [2.11] as the equations of motion for a spherical bubble produced by 227.27 kg. of TNT detonated 45.73 metres below the surface. All of the symbols in the legend for these figures have the same meaning as in Figs. 2-11. It should also be understood that, for the spherical bubble, the effects of drag were ignored unless a value of the drag coefficient C_D is given in the legend. When drag was considered, F_D was given by eq. [2.8]. It should be emphasized that a drag term was incorporated only into the equations of motion for a spherical bubble and never into eqs. [3.43] - [3.46], the equations of motion for a spheroidal bubble.

The behaviour of the spheroidal bubble in Figs. 14-17 was very similar to that in Figs. 2-5. One difference was the close agreement among all four curves for the period of the first bubble oscillation. As well, for the second oscillation, the period predicted by the spheroidal model was closer to that of the spherical model with drag than that which was predicted by the spherical model without drag. This applied in the cases for which radiative energy loss was considered as well as those cases for which it was not. In Figs. 18-21, it can be seen that the peak velocities predicted by the spheroidal models, both with and without radiative energy loss, were in agreement with those predicted by the spherical model with drag, most notably at the first minimum.

It is Fig. 22, however, which demonstrates the accuracy of the spheroidal model. As can be seen, the height above the site of the original explosion predicted by the spheroidal model was in good agreement with that predicted by the spherical model with drag, while that predicted by the spherical model in the absence of drag disagreed with that predicted by the spherical model with drag. Because the drag coefficient used with the spherical model was chosen specifically to force the calculated height to agree with observation, the agreement of the spheroidal model with the spherical model in this case consitutes a verification of the spheroidal model. The agreement was not as good at the second minimum, especially for the spheroidal bubble without energy loss. However, once radiative energy loss was added to the spheroidal model, the curves exhibited close agreement with those for the spherical model with drag.

Figure 23 compares the predicted energy losses of the spherical and spheroidal models. Once again, it can be seen that the inclusion of radiation reaction terms increased the predicted energy loss for a spheroidal bubble, in contrast to the spherical model, for which the addition of reaction terms decreased the energy loss. It is interesting, however, the energy remaining to the spheroidal bubble was greater than that remaining to the spherical bubble when losses from both drag and radiation were included.

VI. CONCLUDING REMARKS

In this work, a Lagrangian for an oscillating ellipsoidal bubble which is also undergoing translational motion has been derived, and equations of motion obtained from it. An expression for the generalised dissipative forces caused by the radiation of sound by the bubble was also found, and incorporated into the equations of motion. This equation was specialised to the case of a spheroidal bubble, and the equations of motion solved for some different charge masses and depths, both with and without the effects of radiation of sound having been included.

By comparison with the results obtained from Taylor's spherical bubble model, it was shown that the spheroidal model retained the successful features of the spherical model, notably the prediction of the bubble's oscillatory period, and reproduced, at least qualitatively, notable features of a real bubble's behaviour, such its flattening near its first minimum, and a slower rise time than that predicted by the spherical model. After the first minimum, the bubble's shape was not as well modelled by a spheroid; however, the results obtained at those times were still superior to those from the spherical model, particularly with respect to the rise time. For the case cited by Hicks (1972), the spheroidal bubble model produced results which were in very close agreement with experimental data. The spherical model was capable of similar agreement only for a limited time and only with the addition of a drag term. The spheroidal model's advantage arises from its reproduction of the height above the explosion site naturally, without the addition of a drag term which must be determined from experimental data for each case. Incidentally, because the spheroidal model ignored hydrodynamic drag completely, and still reproduced the observed behaviour of the bubble, it seems likely that drag is relatively unimportant in determining the bubble's motion; it appears, rather, that the shape of the bubble is the single most important factor.

It appears that the spheroidal model predicted a greater loss of energy in the bubble through the radiation of sound than the spherical model. This was found to be most significant when radiation reaction terms were included in the radiative dissipation function. In contrast to the spherical model, the effect of including radiation reaction terms was to increase the energy loss.

VII. BIBLIOGRAPHY

Cole, R.H. 1948, Underwater Explosions, Princeton University Press, Princeton

Heaton, K.C. 1984, in Transactions of the 2nd Army Conference on Applied Mathematics and Computing, 535, ARO Report 85-1, U.S. Army Research Office, UNCLASSIFIED

Herring, C. 1942, in Underwater Explosion Research, Vol. II, 35 Office of Naval Research, Dept. of the Navy, Washington, D.C., 1950, UNCLASSIFIED

Hicks, A.N. 1972, The Theory of Explosion Induced Whipping Ship Motions, Report no. NCRE/R579, Naval Construction Research Establishment, St. Leonard's Hill, Dunfermline, Fife UNCLASSIFIED

Holt, R.A. 1977, Annual Review of Fluid Mechanics, 9, 187 Pao Alto, California

Landau, L.D. and Lifshitz, E.M. 1966, Fluid Mechanics, Addison-Wesley Inc., Don Mills, Ontario

Milne-Thomson, L.M. 1949, Theoretical Hydrodynamics, Macmillan and Co. Ltd., St. Martin's St., London

Penney, W.G., and Price, A.T. 1942, in Underwater Explosion Research, Vol. II, 145, Office of Naval Research, Dept. of the Navy, Washington, D.C., 1950, UNCLASSIFIED

Shiffman, M. and Friedman, B. 1944, in Underwater Explosion Research, Vol. II, 245, Office of Naval Research, Dept. of the Navy, Washington, D.C., 1950, UNCLASSIFIED

Taylor, Sir G.I. 1942, in The Scientific Paperes of Sir Geoffrey Ingram Taylor, Vol. III, 320, Cambridge University Press, Cambridge 1963

_____1943, in The Scientific Papers of Sir Geoffrey Ingram Taylor, Vol. III, 337, Cambridge University Press, Cambridge 1963

Ward, A.B. 1943, Index 20, cited in Cole (1948)

Figure 1

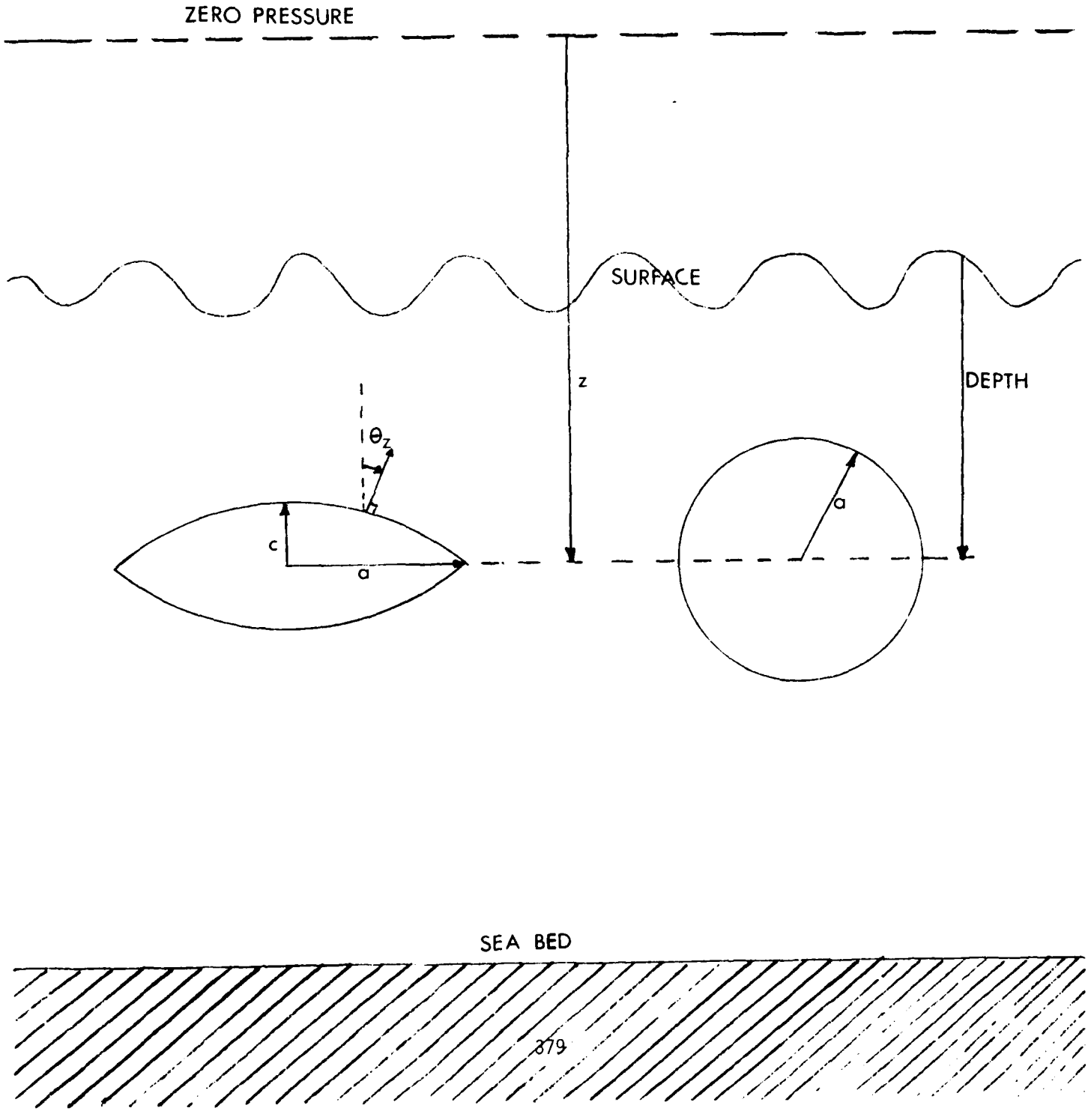

FIGURE 2

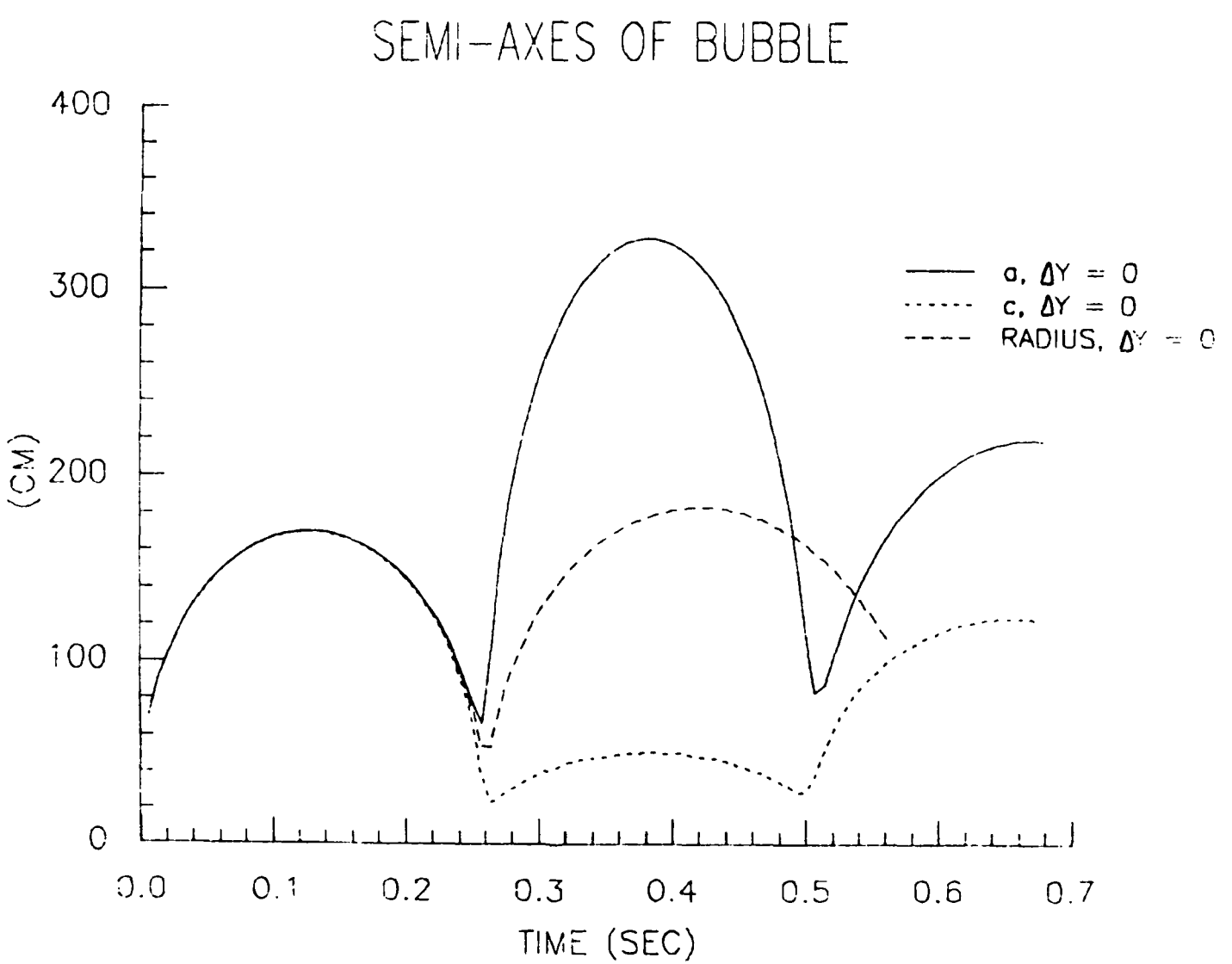
SEMI-AXES OF BUBBLE
400
300
200
100
0
(CM)
a, ΔY = 0
c, ΔY = 0
RADIUS, ΔY = 0
0.0
0.1
0.2
0.3
0.4
0.5
0.6
0.7
TIME (SEC)

FIGURE 3

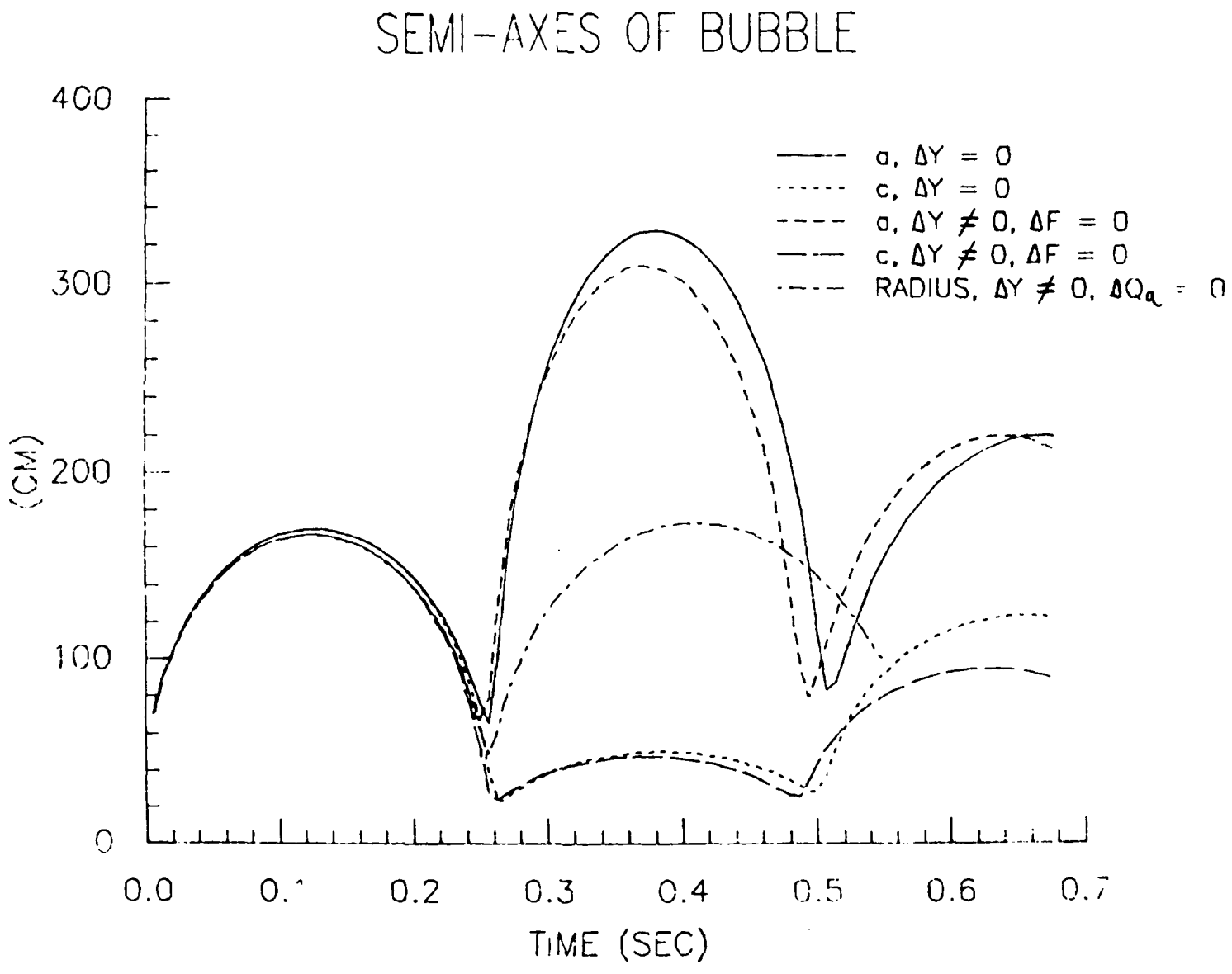
SEMI-AXES OF BUBBLE
400
300
200
100
0
(CM)
0.0
0.1
0.2
0.3
0.4
0.5
0.6
0.7
TIME (SEC)
a, ΔY = 0
c, ΔY = 0
a, ΔY ≠ 0, ΔF = 0
c, ΔY ≠ 0, ΔF = 0
RADIUS, ΔY ≠ 0, ΔQ_a = 0

FIGURE 4

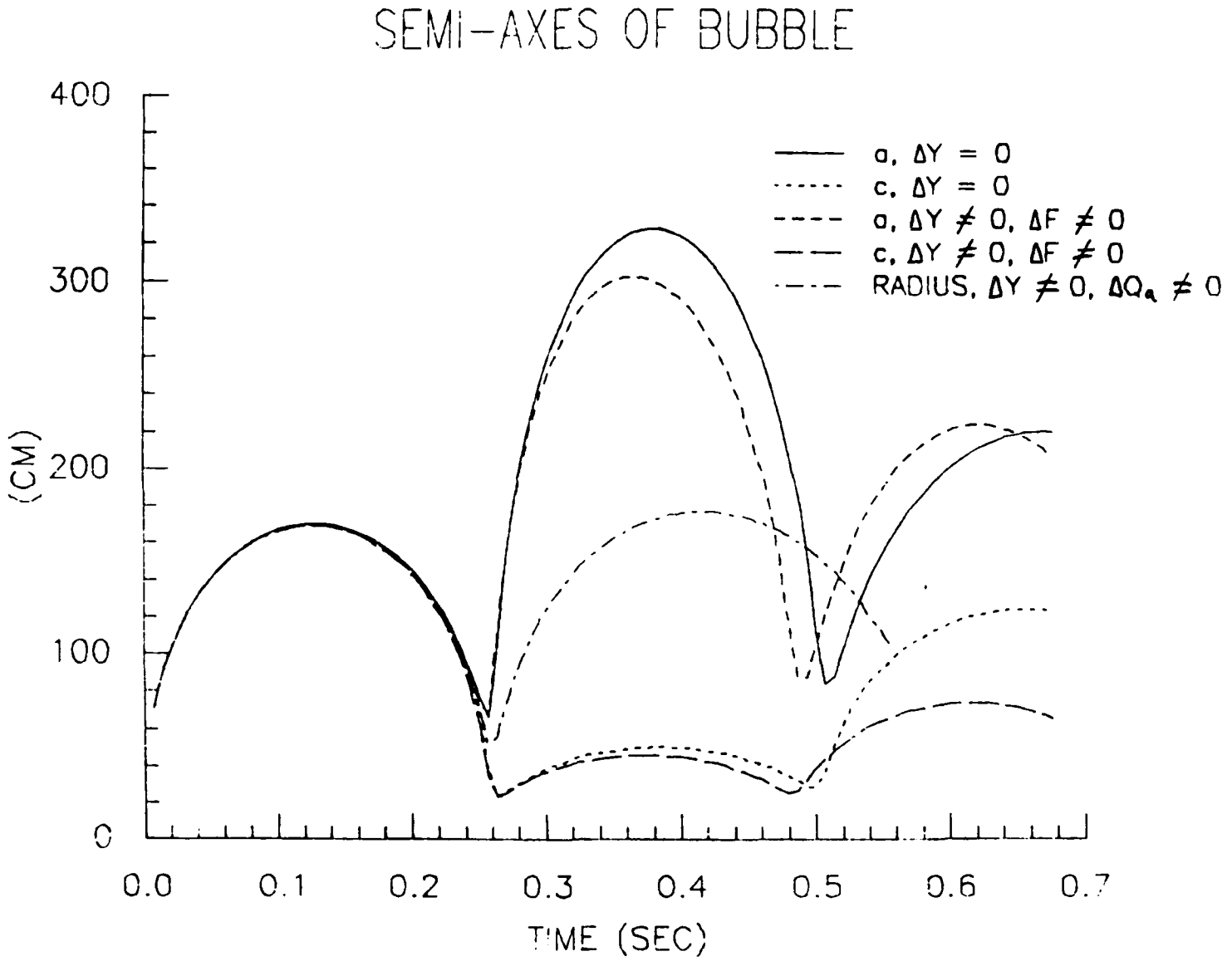
SEMI-AXES OF BUBBLE
400
300
200
100
0
(CM)
0.0
0.1
0.2
0.3
0.4
0.5
0.6
0.7
TIME (SEC)
a, ΔY = 0
c, ΔY = 0
a, ΔY ≠ 0, ΔF ≠ 0
c, ΔY ≠ 0, ΔF ≠ 0
RADIUS, ΔY ≠ 0, ΔQ_a ≠ 0

FIGURE 5

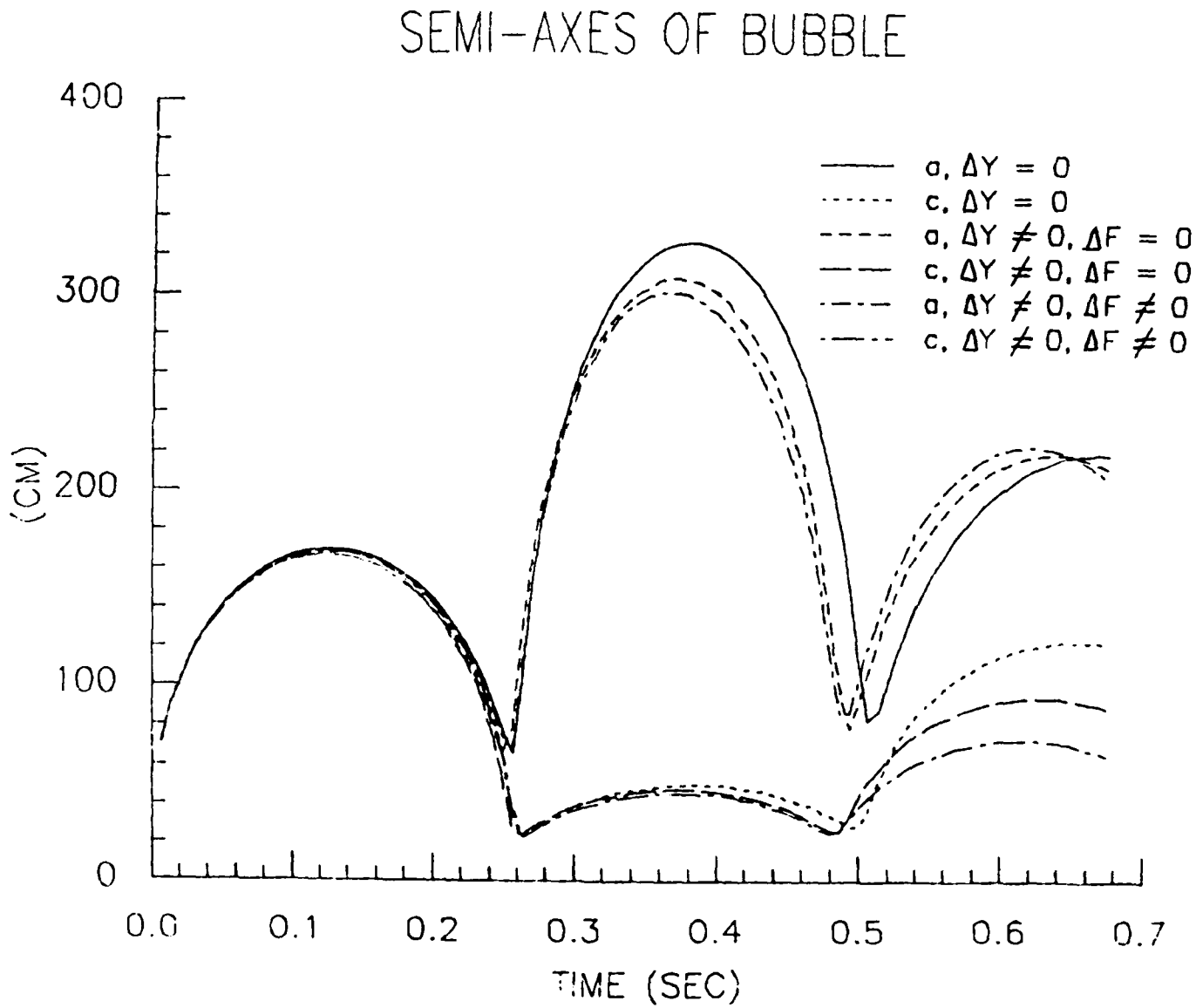
SEMI-AXES OF BUBBLE
400
300
200
100
0
(CM)
0.0
0.1
0.2
0.3
0.4
0.5
0.6
0.7
TIME (SEC)
a, ΔY = 0
c, ΔY = 0
a, ΔY ≠ 0, ΔF = 0
c, ΔY ≠ 0, ΔF = 0
a, ΔY ≠ 0, ΔF ≠ 0
c, ΔY ≠ 0, ΔF ≠ 0

FIGURE 6

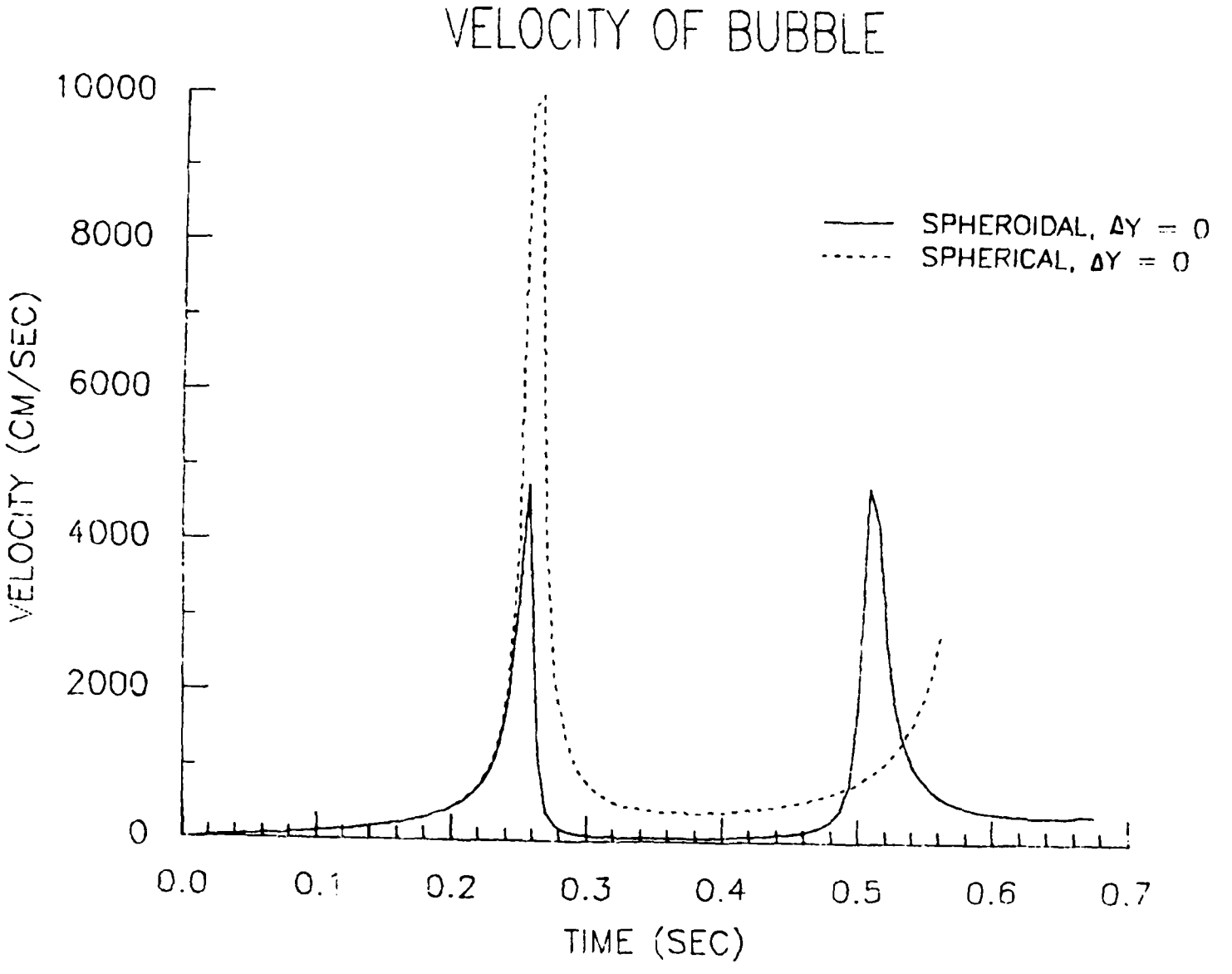
VELOCITY OF BUBBLE
10000
8000
6000
4000
2000
0
VELOCITY (CM/SEC)
0.0
0.1
0.2
0.3
0.4
0.5
0.6
0.7
TIME (SEC)
SPHEROIDAL, ΔY = 0
SPHERICAL, ΔY = 0

FIGURE 7

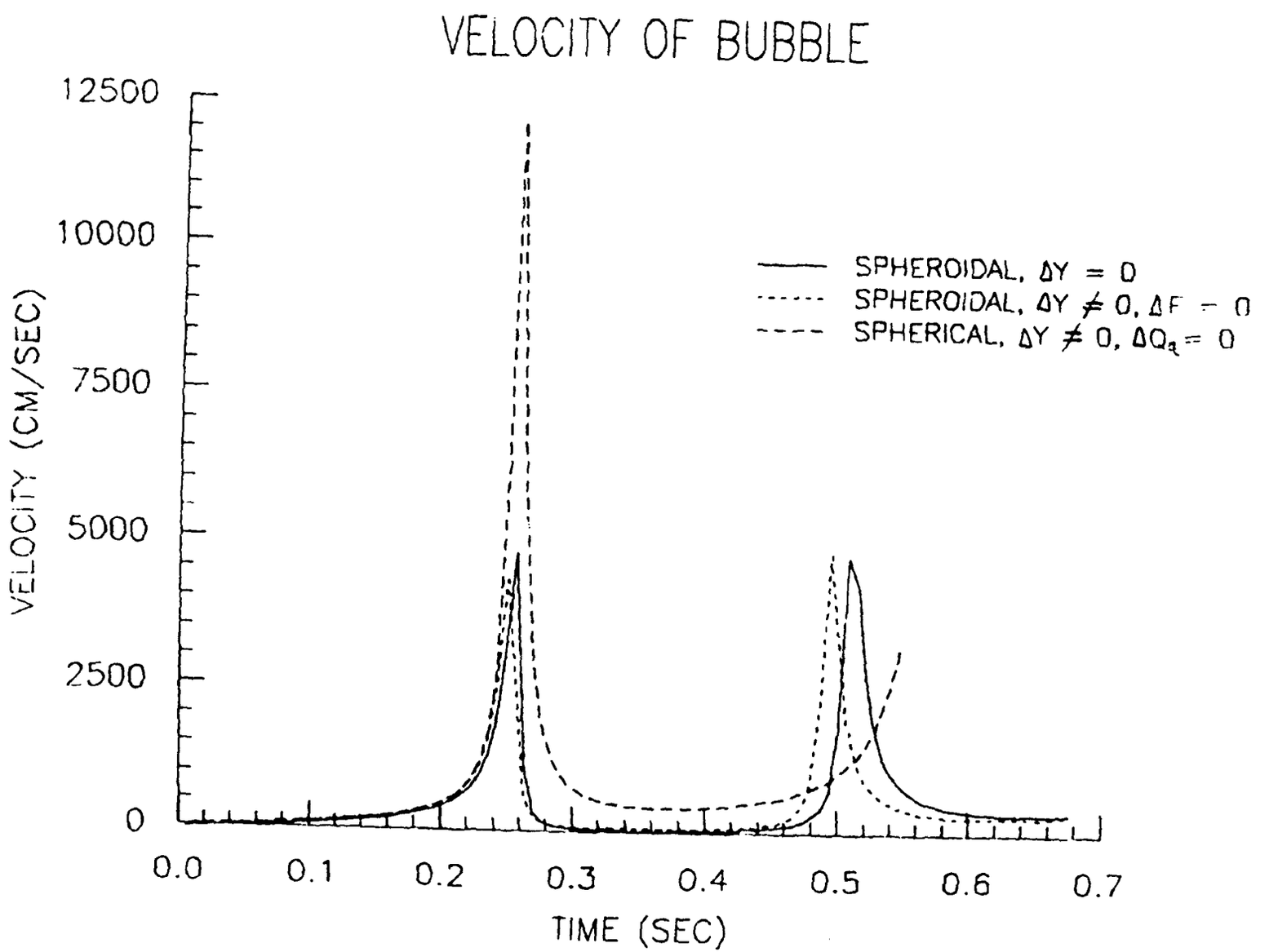
VELOCITY OF BUBBLE
12500
10000
7500
5000
2500
0
VELOCITY (CM/SEC)
0.0
0.1
0.2
0.3
0.4
0.5
0.6
0.7
TIME (SEC)
SPHEROIDAL, ΔY = 0
SPHEROIDAL, ΔY ≠ 0, ΔF = 0
SPHERICAL, ΔY ≠ 0, ΔQ = 0

FIGURE 8

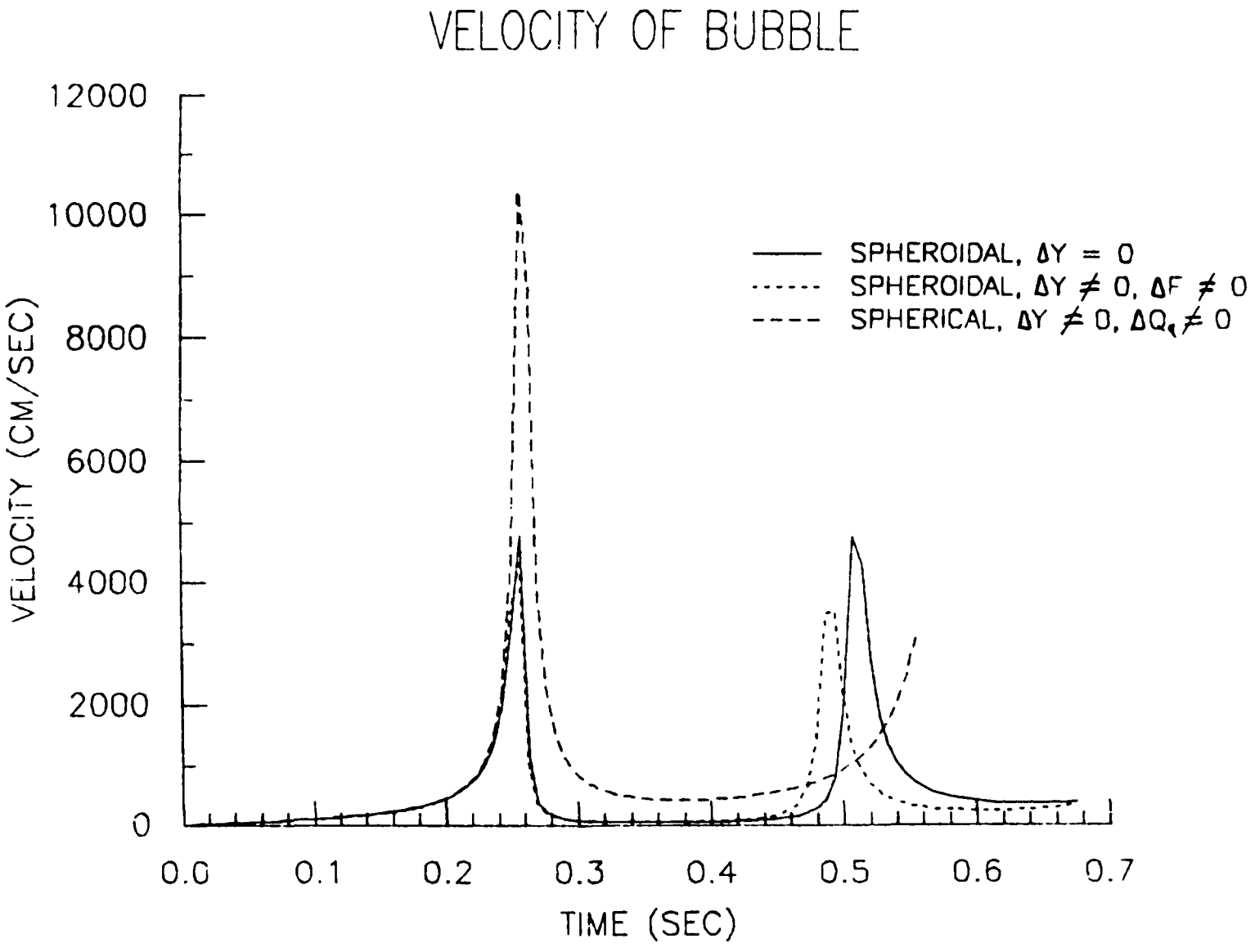
VELOCITY OF BUBBLE
12000
10000
8000
6000
4000
2000
0
VELOCITY (CM/SEC)
0.0
0.1
0.2
0.3
0.4
0.5
0.6
0.7
TIME (SEC)
SPHEROIDAL, ΔY = 0
SPHEROIDAL, ΔY ≠ 0, ΔF ≠ 0
SPHERICAL, ΔY ≠ 0, ΔQ ≠ 0

FIGURE 9

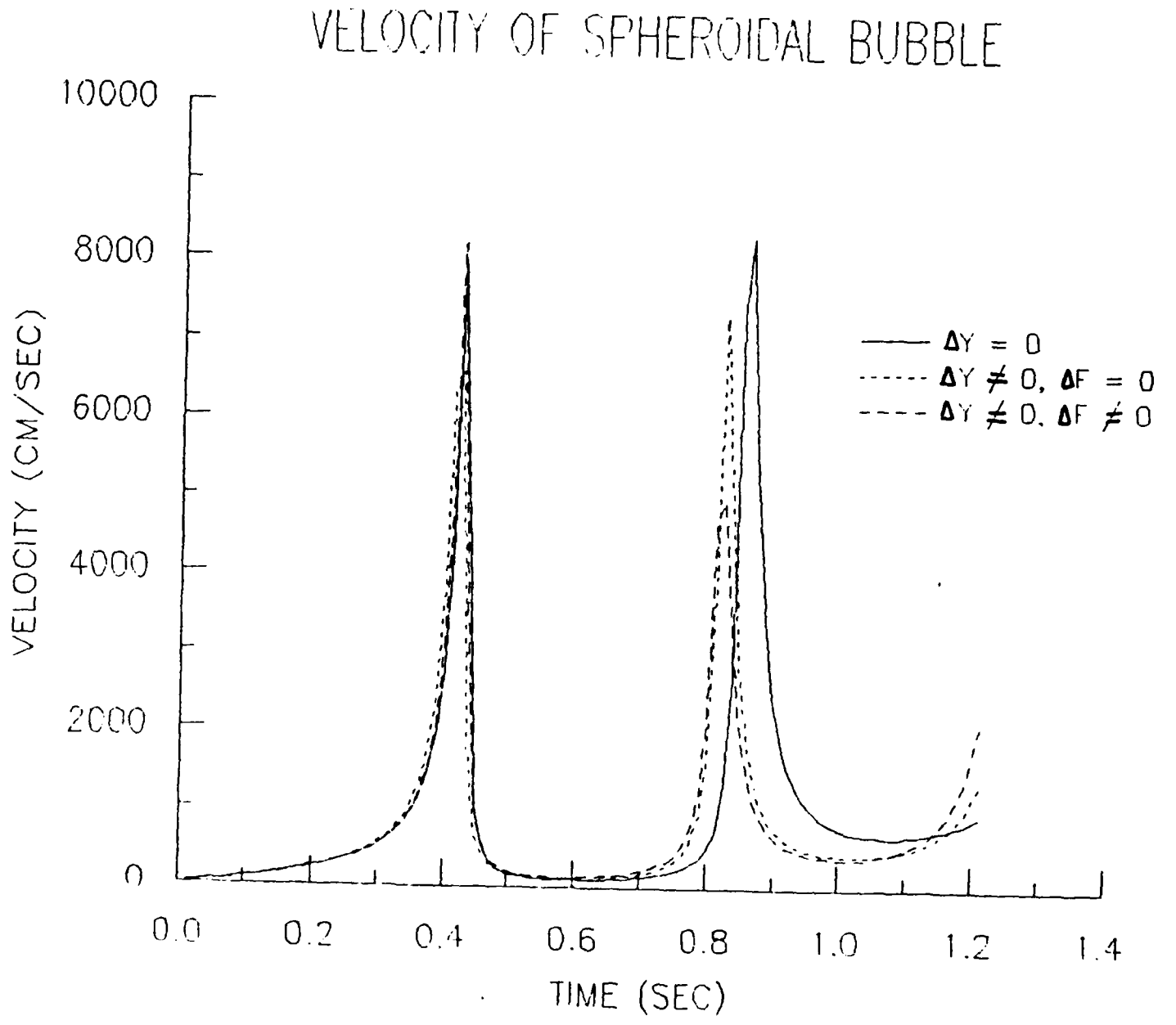
VELOCITY OF SPHEROIDAL BUBBLE
VELOCITY (CM/SEC)
10000
8000
6000
4000
2000
0
0.0
0.2
0.4
0.6
0.8
1.0
1.2
1.4
TIME (SEC)
ΔY = 0
ΔY ≠ 0, ΔF = 0
ΔY ≠ 0, ΔF ≠ 0

FIGURE 10

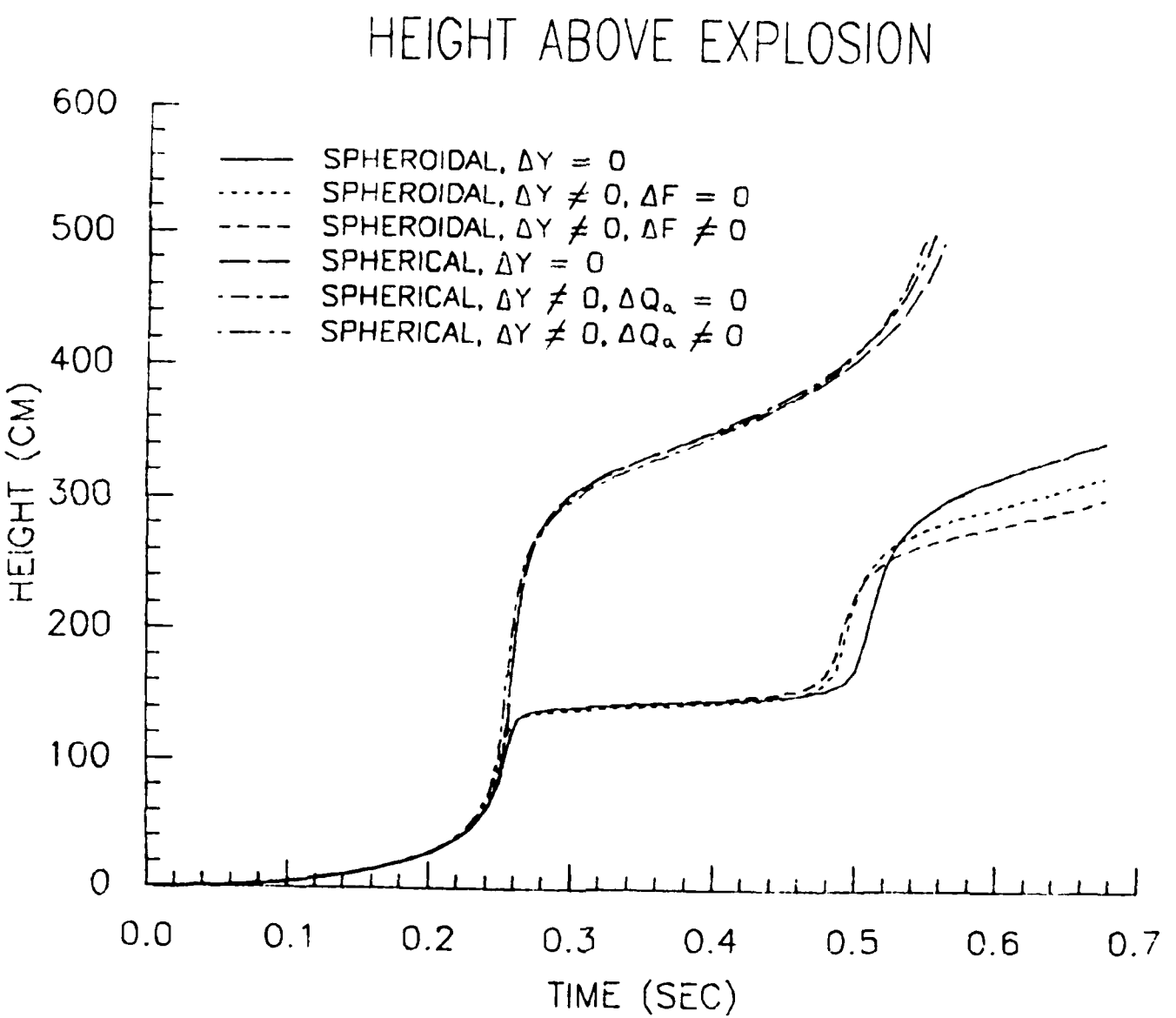
HEIGHT ABOVE EXPLOSION
SPHEROIDAL, ΔY = 0
SPHEROIDAL, ΔY ≠ 0, ΔF = 0
SPHEROIDAL, ΔY ≠ 0, ΔF ≠ 0
SPHERICAL, ΔY = 0
SPHERICAL, ΔY ≠ 0, ΔQa = 0
SPHERICAL, ΔY ≠ 0, ΔQa ≠ 0
HEIGHT (CM)
600
500
400
300
200
100
0
0.0
0.1
0.2
0.3
0.4
0.5
0.6
0.7
TIME (SEC)

FIGURE 11

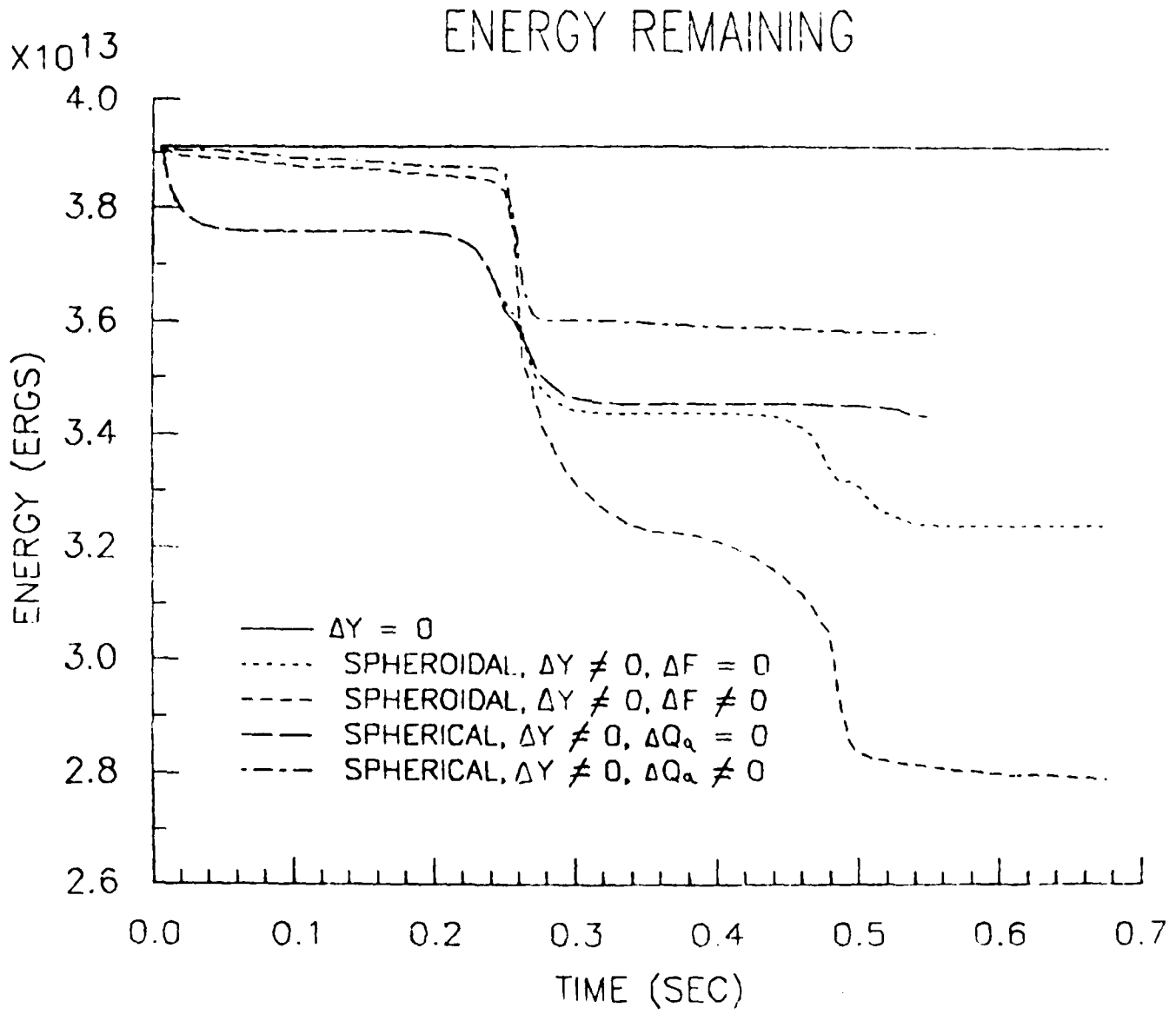
ENERGY REMAINING
X10^13
4.0
3.8
3.6
3.4
3.2
3.0
2.8
2.6
ENERGY (ERGS)
0.0
0.1
0.2
0.3
0.4
0.5
0.6
0.7
TIME (SEC)
ΔY = 0
SPHEROIDAL, ΔY ≠ 0, ΔF = 0
SPHEROIDAL, ΔY ≠ 0, ΔF ≠ 0
SPHERICAL, ΔY ≠ 0, ΔQa = 0
SPHERICAL, ΔY ≠ 0, ΔQa ≠ 0

FIGURE 12

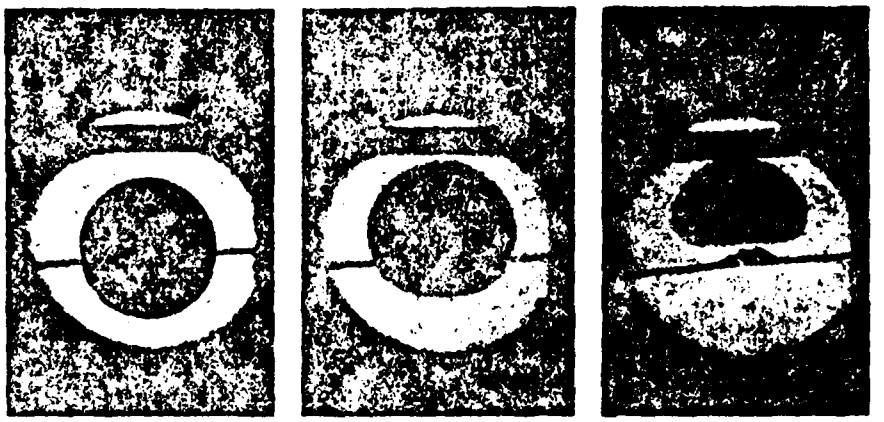

Fig. 4 Fig. 5 Fig. 6

Figs. 4–6. Photographs of bubbles in oil under vacuum, showing how the bubble becomes distorted as its age increases. Fig. 4. Spherical bubble, age 25 msec. Fig. 5. Bubble with pronounced flattening on underside, age 50 msec. Fig. 6. Mushroom shaped bubble, age 80 msec.

(*facing p.* 346)

Evolution in time of a bubble in oil

(photograph from Taylor (1943))

FIGURE 13

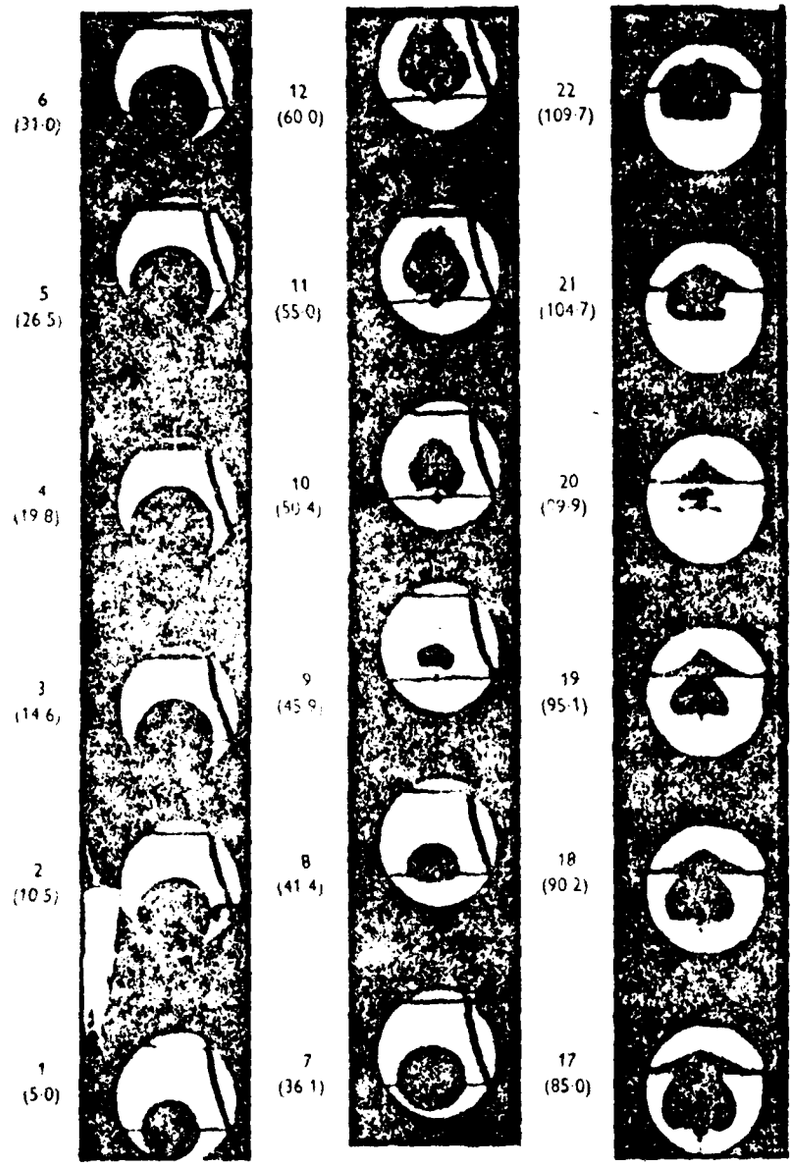

Fig. 8. Photographs of bubble in oil taken with a revolving drum camera. Upper number: identification number of photograph. Lower number in parenthesis: age of bubble in milliseconds.

Evolution in time of a bubble in oil

(photograph from Taylor (1943))

FIGURE 14

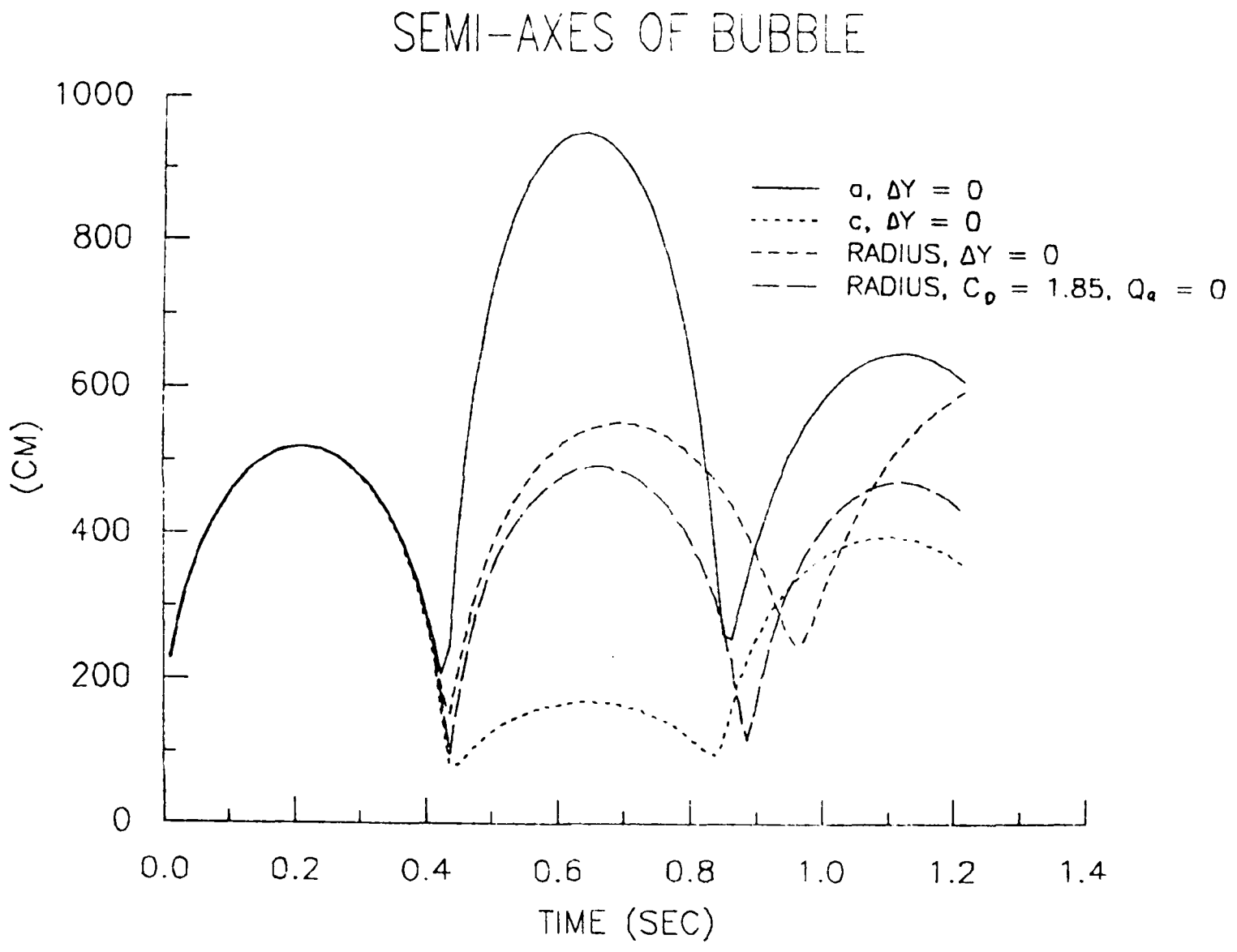
SEMI-AXES OF BUBBLE
1000
800
600
400
200
0
(CM)
0.0
0.2
0.4
0.6
0.8
1.0
1.2
1.4
TIME (SEC)
a, ΔY = 0
c, ΔY = 0
RADIUS, ΔY = 0
RADIUS, C_D = 1.85, Q_a = 0

FIGURE 15

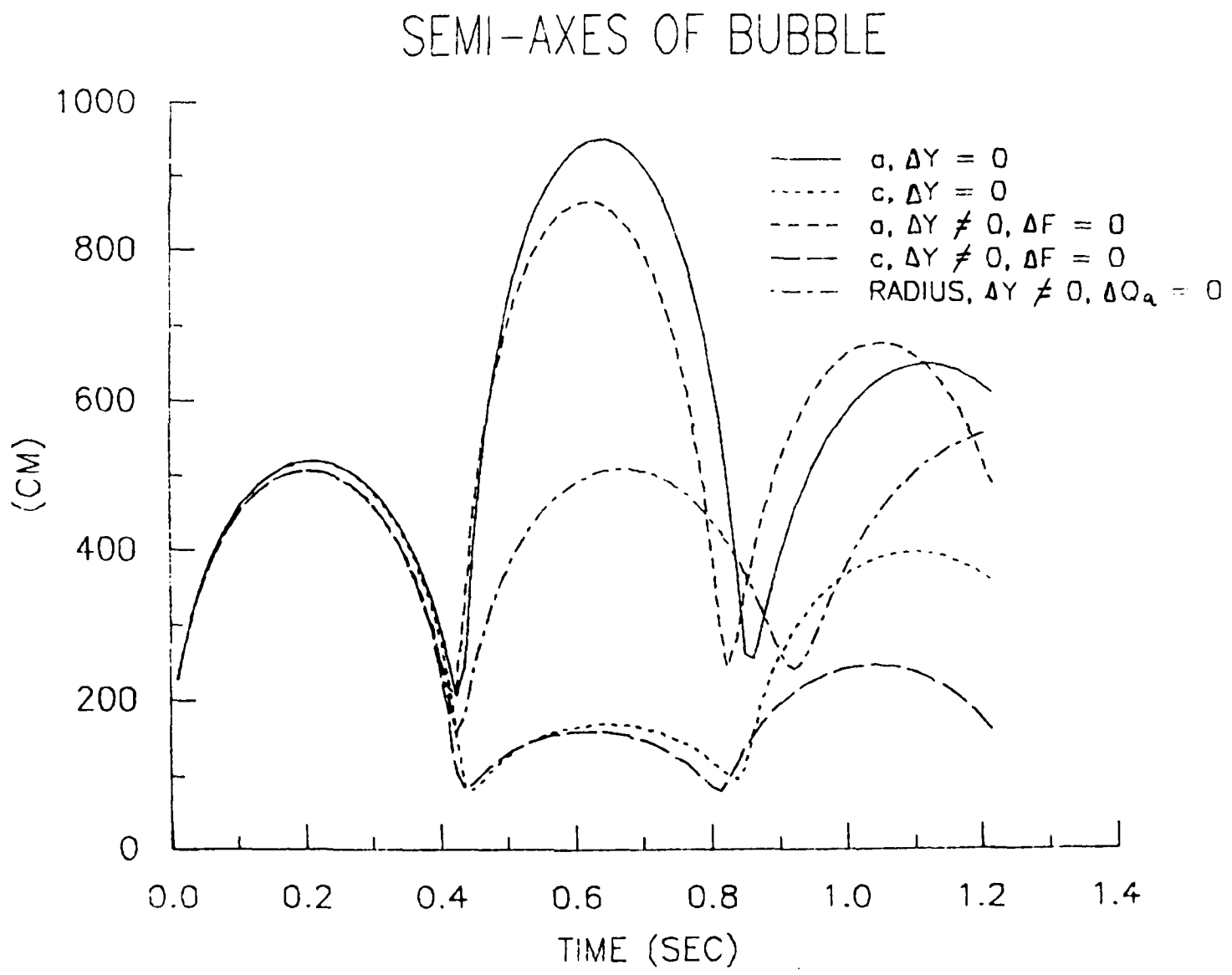
SEMI-AXES OF BUBBLE
1000
800
600
400
200
0
(CM)
0.0
0.2
0.4
0.6
0.8
1.0
1.2
1.4
TIME (SEC)
a, ΔY = 0
c, ΔY = 0
a, ΔY ≠ 0, ΔF = 0
c, ΔY ≠ 0, ΔF = 0
RADIUS, ΔY ≠ 0, ΔQa = 0

FIGURE 16

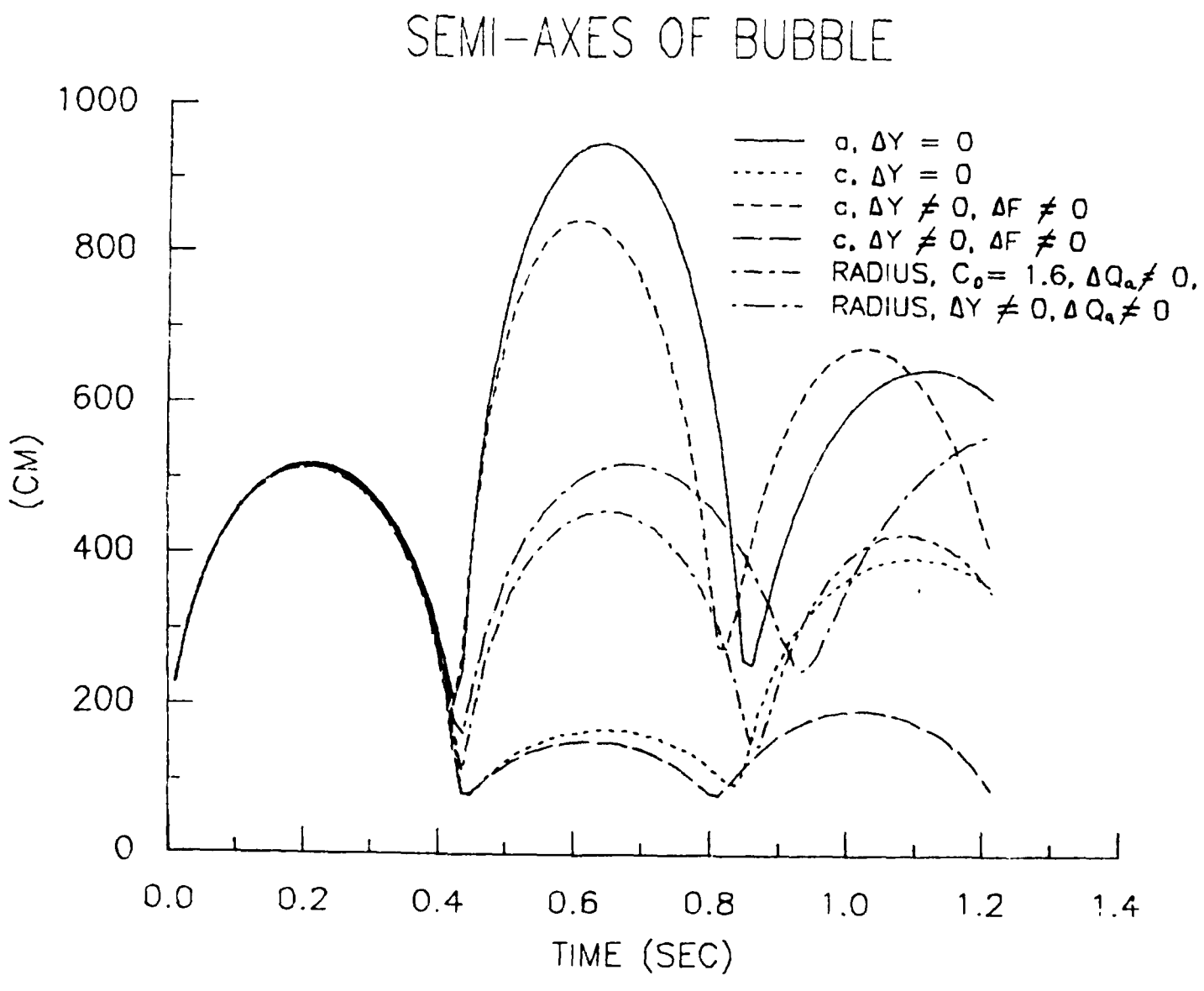
SEMI-AXES OF BUBBLE
1000
800
600
400
200
0
(CM)
0.0
0.2
0.4
0.6
0.8
1.0
1.2
1.4
TIME (SEC)
a, ΔY = 0
c, ΔY = 0
c, ΔY ≠ 0, ΔF ≠ 0
c, ΔY ≠ 0, ΔF ≠ 0
RADIUS, C₀= 1.6, ΔQₐ≠ 0,
RADIUS, ΔY ≠ 0, ΔQₐ≠ 0

FIGURE 17

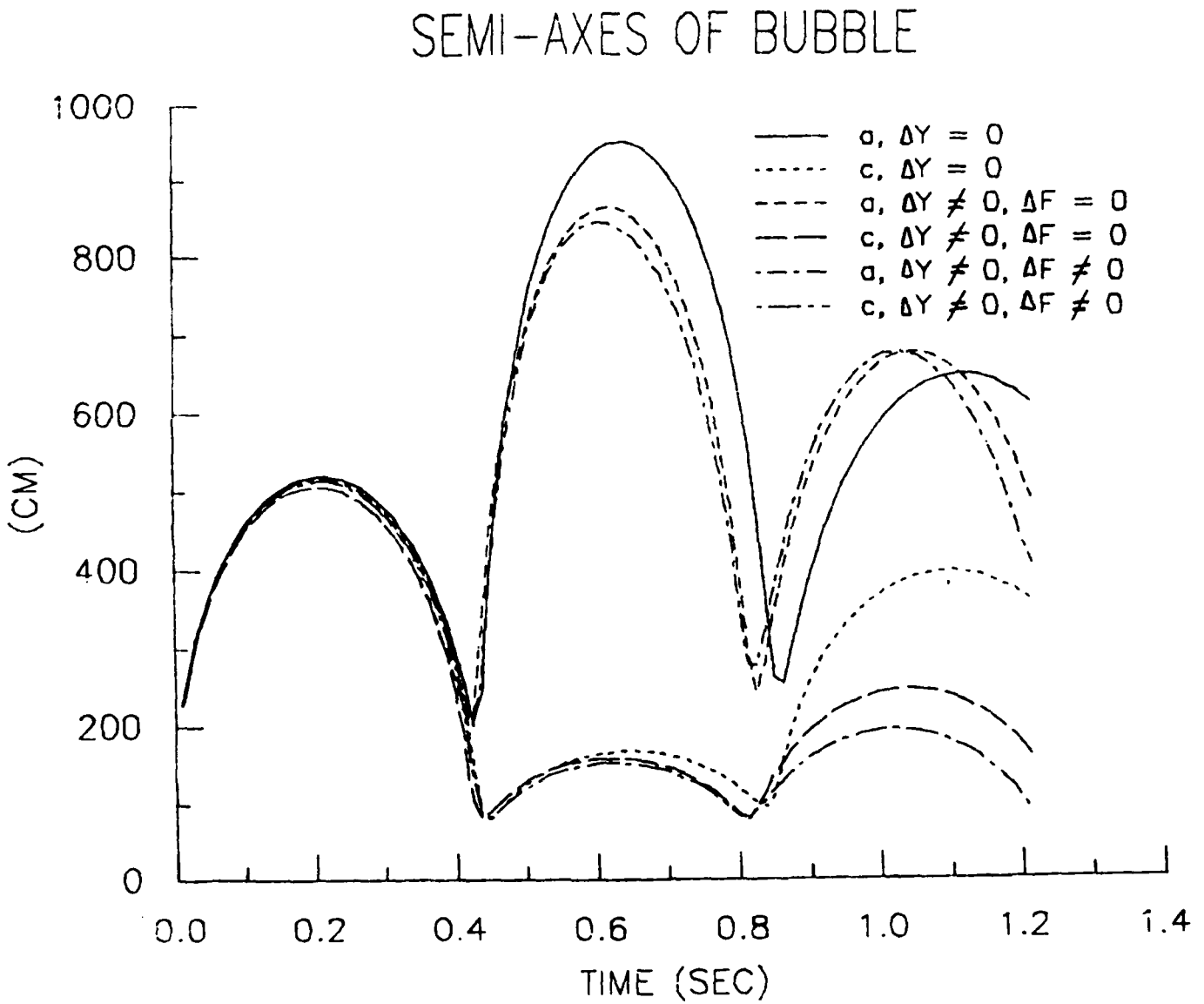
SEMI-AXES OF BUBBLE
1000
800
600
400
200
0
(CM)
0.0
0.2
0.4
0.6
0.8
1.0
1.2
1.4
TIME (SEC)
a, ΔY = 0
c, ΔY = 0
a, ΔY ≠ 0, ΔF = 0
c, ΔY ≠ 0, ΔF = 0
a, ΔY ≠ 0, ΔF ≠ 0
c, ΔY ≠ 0, ΔF ≠ 0

FIGURE 18

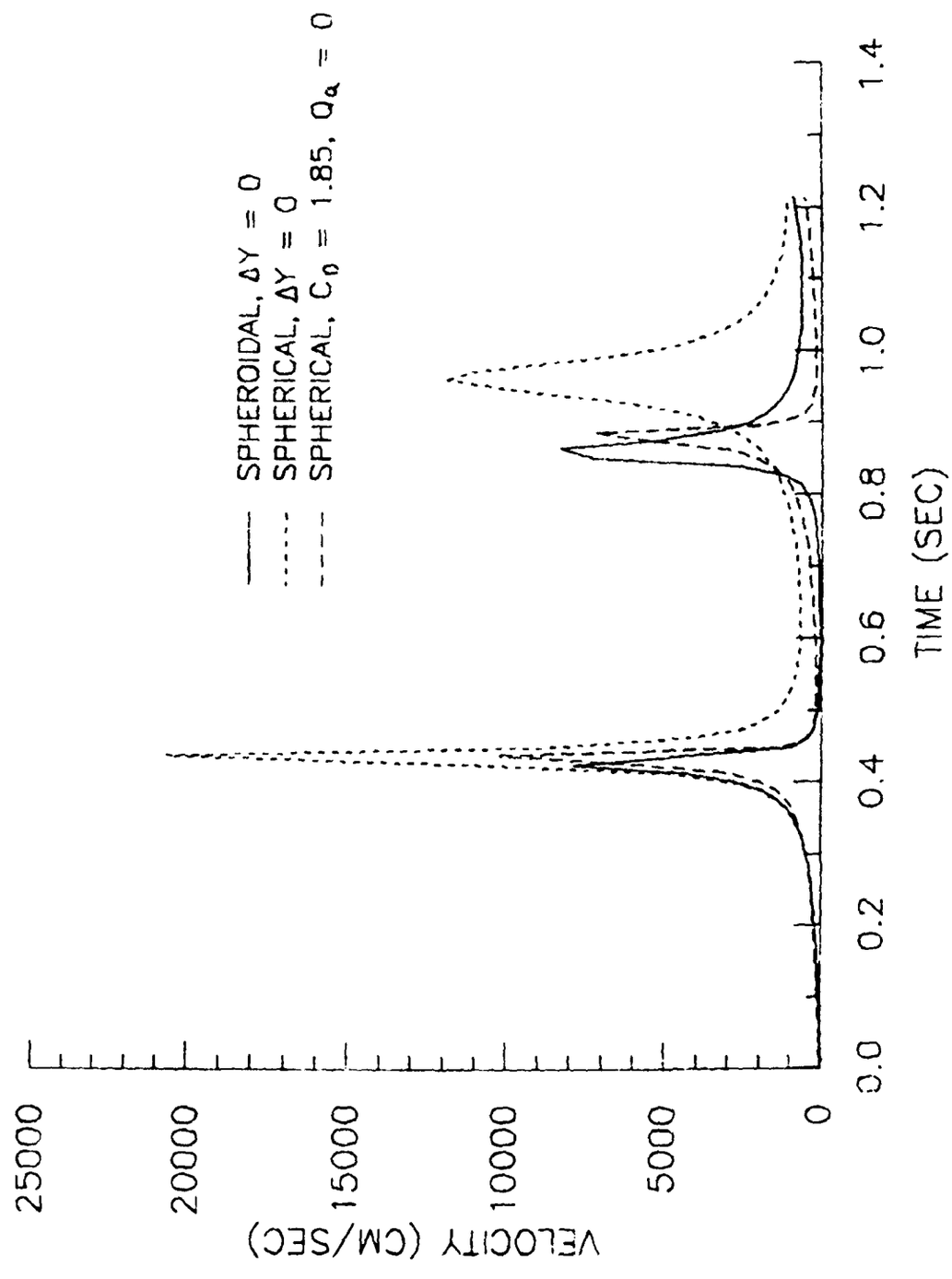
VELOCITY OF BUBBLE
SPHEROIDAL, ΔY = 0
SPHERICAL, ΔY = 0
SPHERICAL, C_0 = 1.85, Q_a = 0
VELOCITY (CM/SEC)
25000
20000
15000
10000
5000
0
0.0
0.2
0.4
0.6
0.8
1.0
1.2
1.4
TIME (SEC)

FIGURE 19

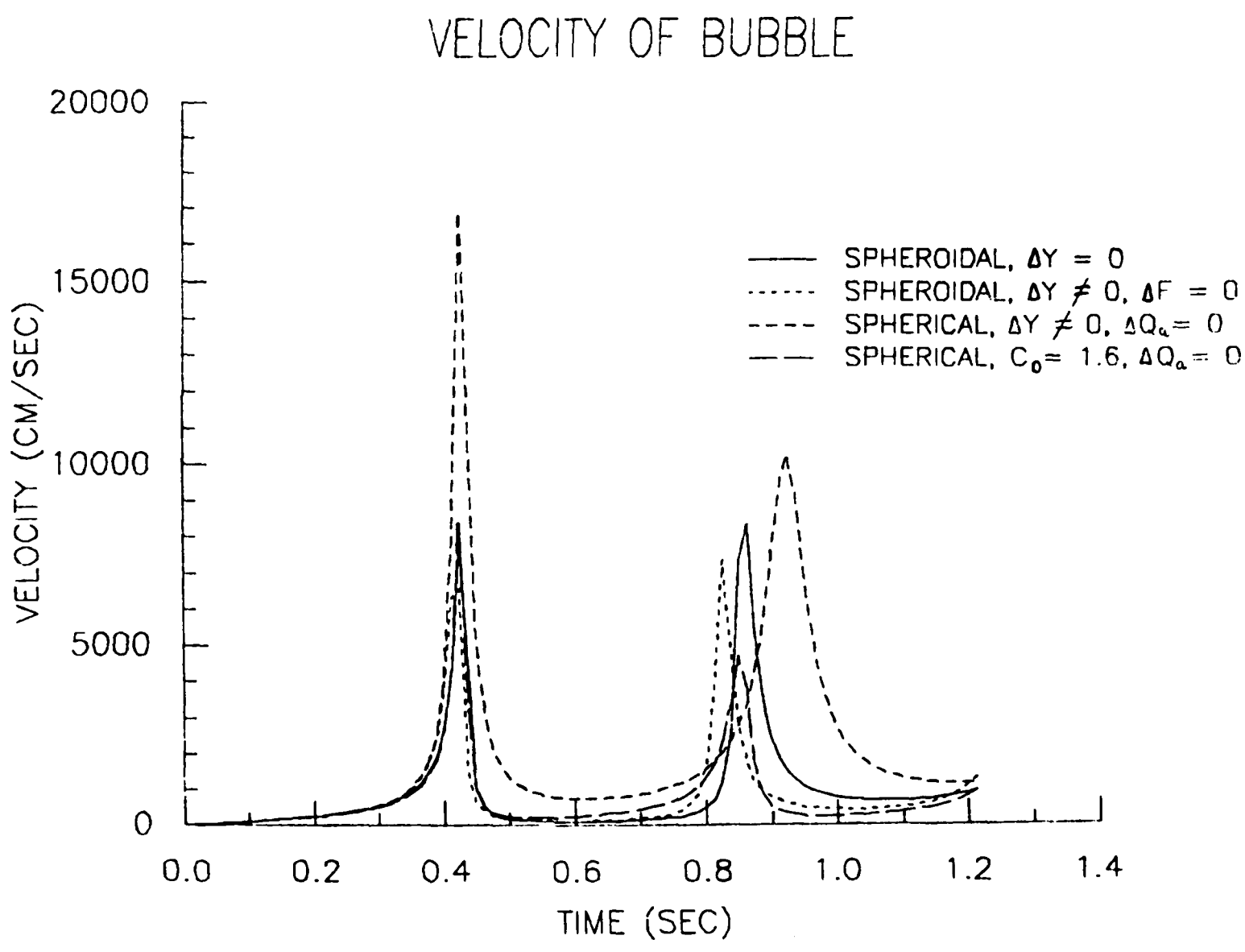
VELOCITY OF BUBBLE
20000
15000
10000
5000
0
VELOCITY (CM/SEC)
0.0
0.2
0.4
0.6
0.8
1.0
1.2
1.4
TIME (SEC)
SPHEROIDAL, ΔY = 0
SPHEROIDAL, ΔY ≠ 0, ΔF = 0
SPHERICAL, ΔY ≠ 0, ΔQa = 0
SPHERICAL, C0 = 1.6, ΔQa = 0

FIGURE 20

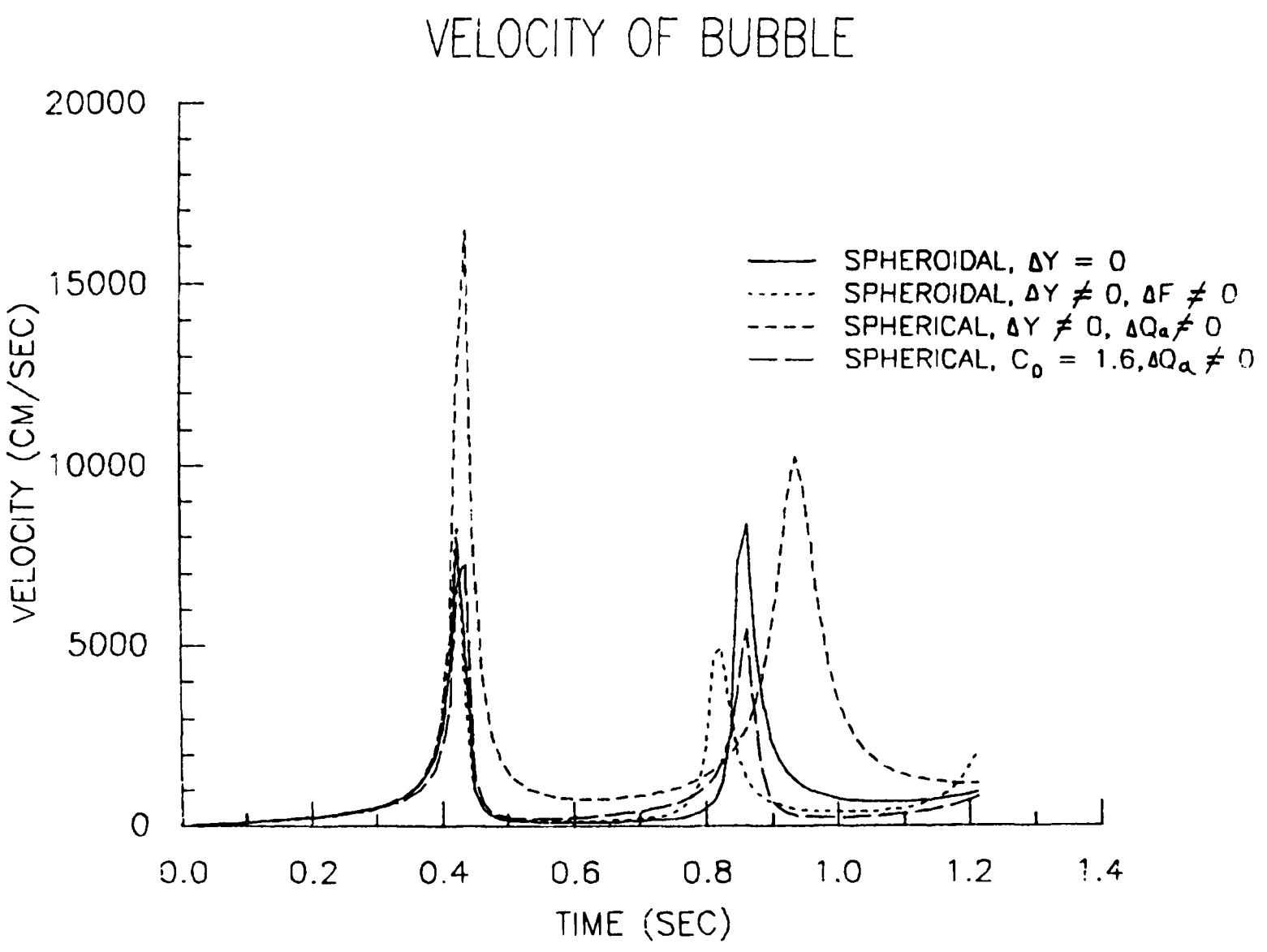
VELOCITY OF BUBBLE
20000
15000
10000
5000
0
VELOCITY (CM/SEC)
0.0
0.2
0.4
0.6
0.8
1.0
1.2
1.4
TIME (SEC)
SPHEROIDAL, ΔY = 0
SPHEROIDAL, ΔY ≠ 0, ΔF ≠ 0
SPHERICAL, ΔY ≠ 0, ΔQa ≠ 0
SPHERICAL, C0 = 1.6, ΔQa ≠ 0

FIGURE 21

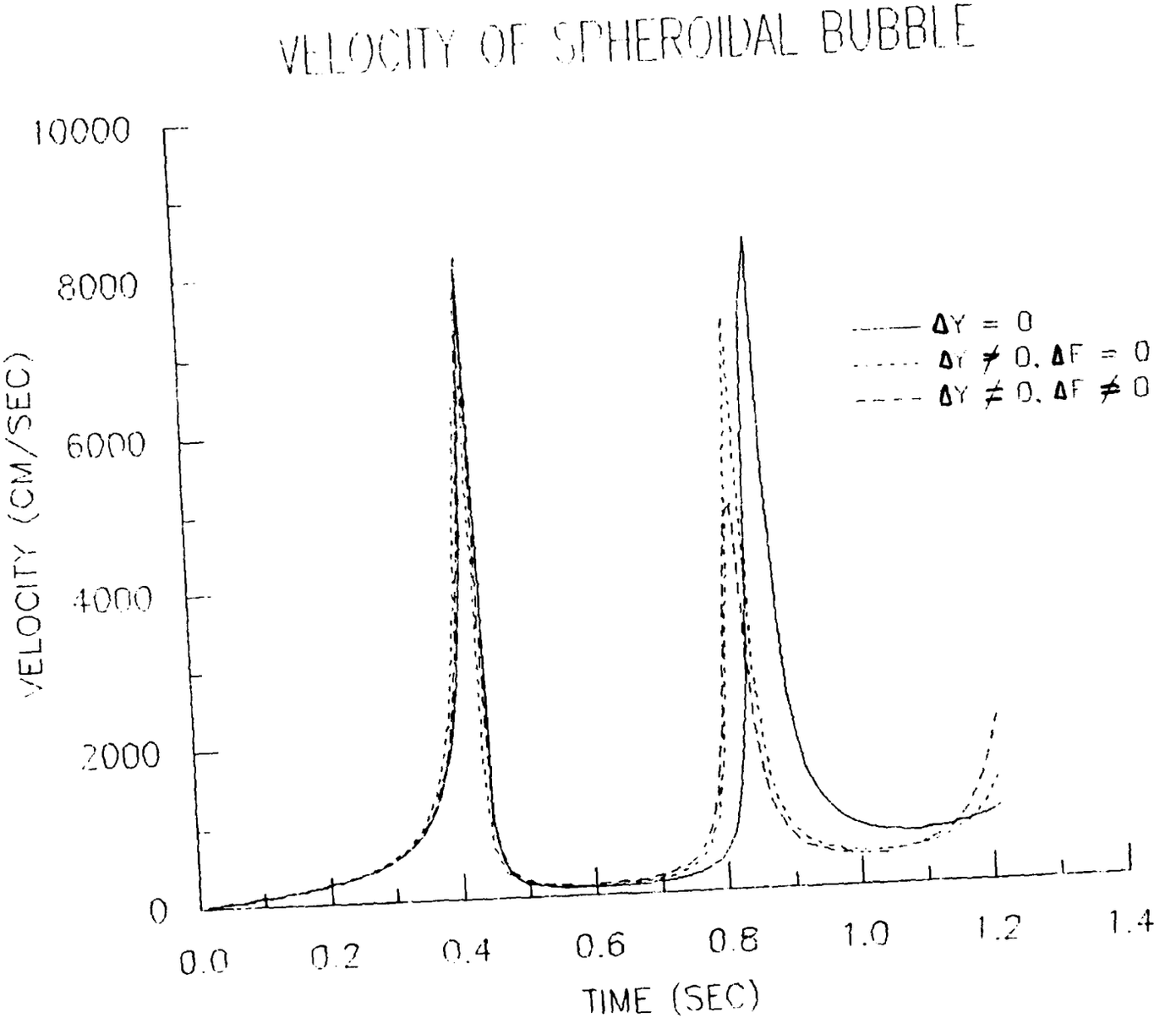
VELOCITY OF SPHEROIDAL BUBBLE
10000
8000
6000
4000
2000
0
VELOCITY (CM/SEC)
0.0
0.2
0.4
0.6
0.8
1.0
1.2
1.4
TIME (SEC)
ΔY = 0
ΔY ≠ 0, ΔF = 0
ΔY ≠ 0, ΔF ≠ 0

FIGURE 22

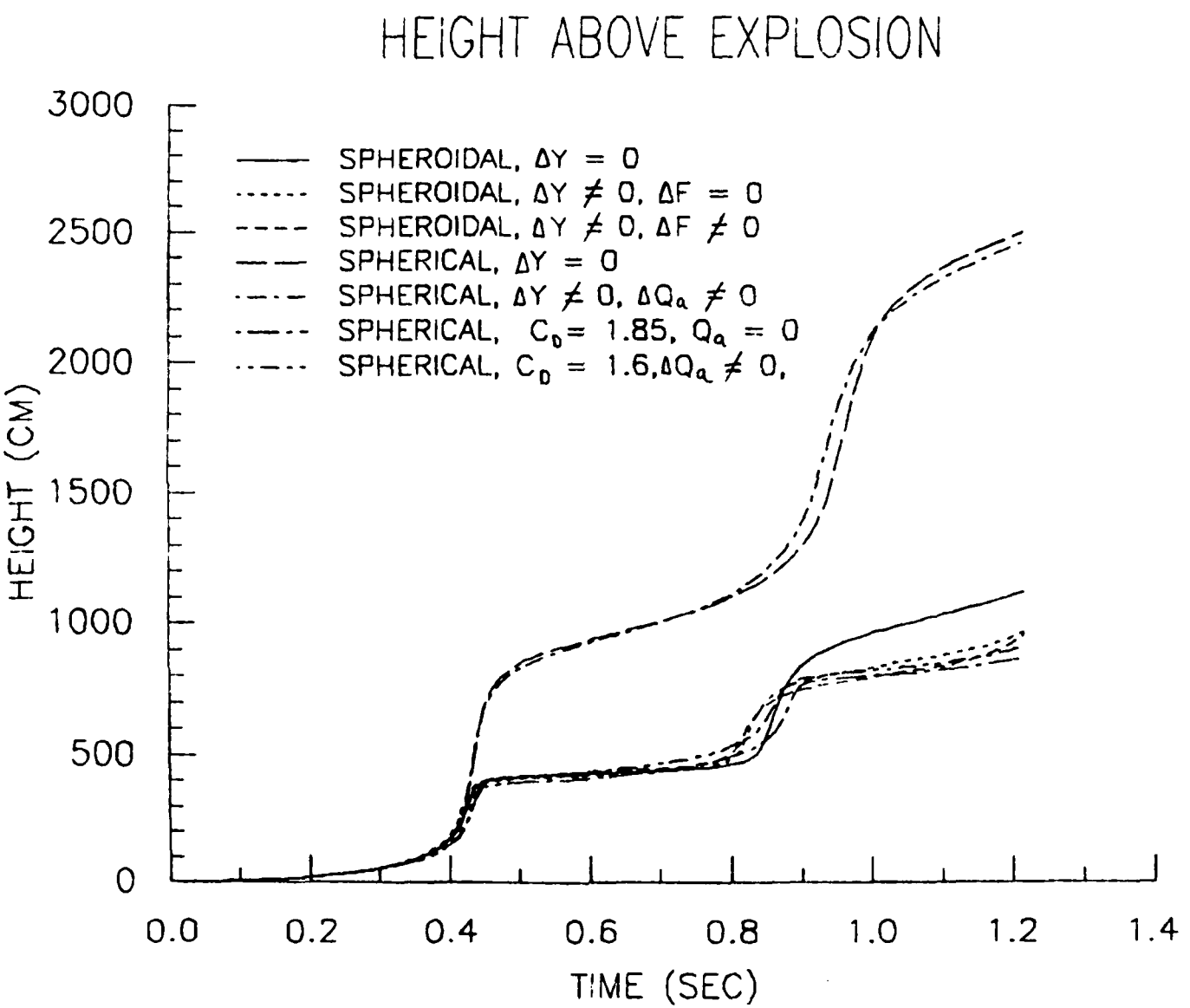
HEIGHT ABOVE EXPLOSION
SPHEROIDAL, ΔY = 0
SPHEROIDAL, ΔY ≠ 0, ΔF = 0
SPHEROIDAL, ΔY ≠ 0, ΔF ≠ 0
SPHERICAL, ΔY = 0
SPHERICAL, ΔY ≠ 0, ΔQa ≠ 0
SPHERICAL, C0 = 1.85, Qa = 0
SPHERICAL, C0 = 1.6, ΔQa ≠ 0,
HEIGHT (CM)
3000
2500
2000
1500
1000
500
0
0.0
0.2
0.4
0.6
0.8
1.0
1.2
1.4
TIME (SEC)

FIGURE 23

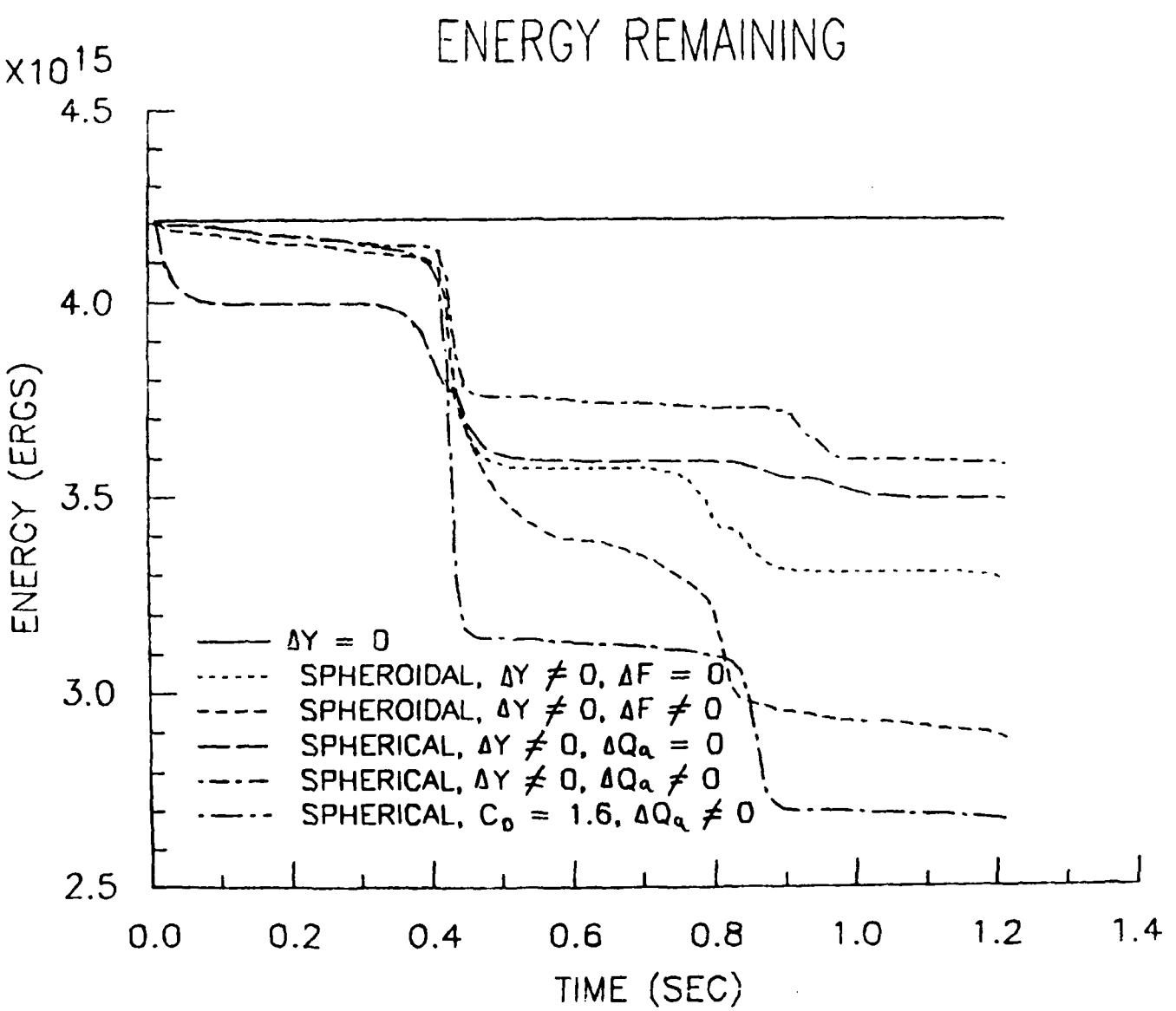
ENERGY REMAINING
X10^15
4.5
4.0
3.5
3.0
2.5
ENERGY (ERGS)
0.0
0.2
0.4
0.6
0.8
1.0
1.2
1.4
TIME (SEC)
ΔY = 0
SPHEROIDAL, ΔY ≠ 0, ΔF = 0
SPHEROIDAL, ΔY ≠ 0, ΔF ≠ 0
SPHERICAL, ΔY ≠ 0, ΔQa = 0
SPHERICAL, ΔY ≠ 0, ΔQa ≠ 0
SPHERICAL, C0 = 1.6, ΔQa ≠ 0

END

FILMED

5-86

DTIC